INDIUM TIN OXIDE (ITO) COATING ON CYLINDRICAL SURFACES: ELECTRICAL AND STRUCTURAL CHARACTERIZATION

A Thesis Submitted
To the graduate School of Engineering and Sciences of
Izmir Institute of Technology
in Partial Fulfillment of Requirement for Degree of

MASTER OF SCIENCE

in Physics

by

Halil ARSLAN

October 2015

IZMIR

We approve the thesis of **Halil ARSLAN**

Examine Committee Members:

Prof. Dr. Lütfi ÖZYÜZER
Department of Physics, Izmir Institute of Technology

Asst. Prof. Dr. Enver TARHAN
Department of Physics, Izmir Institute of Technology

Prof. Dr. Aysun AKŞİT
Department of Textile Engineering, Dokuz Eylül University

Prof. Dr. Şerife Hanım YALÇIN
Department of Chemistry, Izmir Institute of Technology

Asst. Prof. Dr. Bengi KUTLU
Department of Textile Engineering, Dokuz Eylül University

23 October 2015

Prof. Dr. Lütfi ÖZYÜZER
Supervisor, Department of Physics,
Izmir Institute of Technology

Asst. Prof. Dr. Gürcan ARAL
Co-Supervisor, Department of Physics,
Izmir Institute of Technology

Prof. Dr. Nejat BULUT
Head of the Department of physics

Prof. Dr. Bilge KARAÇALI
Dean of the Graduate School of
Engineering and Sciences

ACKNOWLEDGEMENTS

I would never have been able to finish my dissertation without the guidance of my committee members, help from friends, and support from my family, Hakan ALABOZ and Kagan AYDIN.

First of all I would like to thank my supervisor Prof. Dr. Lutfi OZYUZER for his excellent guidance, caring, patience, and providing me with an excellent atmosphere for doing researches throughout the projects.

Many thanks must go to my co-advisor Asst. Prof. Dr. Gurcan ARAL for his advice, which is beyond price.

The thanks should go to Prof. Dr. Aysun AKSIT and Asst. Prof. Dr. Bengi KUTLU of Dokuz Eylül University for their valuable comments on flexible electronics. I would also like to thank Ph.D. Candidate Esra TOPEL of Dokuz Eylül who helped me during my thesis.

I also extend my thanks to all former colleagues from Izmir Institute of Technology and our group members, I also want to thank Onur Rauf YILMAZ for his sincereness. I would thank to Sena GULEN and Hurriyet YUCE who helped me during my thesis. Adnan TASDEMIR and Tugce SEMERCI are the ones who deserve special thanks due to their kindly-hearted.

I would like to thank Hakan ALABOZ, who as a good friend, was always willing to help and give his best suggestions. It would not have been a bright laboratory without him.

I would also like to acknowledge that this research was partially supported by TUBITAK 213M282 and special thanks must go to Teknoma Technological Materials Company to let us to study this great research.

Finally, there is no correct words to explain my family contribution to my education and explain their love and express my thanks for their helps.

ABSTRACT

INDIUM TIN OXIDE (ITO) COATING ON CYLINDRICAL SURFACES: ELECTRICAL AND STRUCTURAL CHARACTERIZATION

Optical transparent conductive oxides (TCOs) which were discovered in the first quarter of twentieth century, and which belong to the class of semiconductor elements, are the constituent of today's and future technology thanks to the high optical transparency (≥ % 85) they have in the visible region (390- 700 nm), and to the low electrical resistivity they have (10^{-4} ohm.cm). One of the most common usage of optical transparent conductive oxides; which have a quite extensive application area from transistors to solar panels, from flexible screens to OLEDs; is the textile materials known as smart clothes. The use of TCOs in textile materials, generally occurs by means of electrochromic structures that have the feature of changing color. In the most general sense, electrochromic structures can be defined as the materials that change their colors, which they gain thanks to reduction and oxidation reactions under a low potential difference of 1.5 – 5V, as a transition from one color state to another or from colorless state to color state. Even though they differ according to their area of utilization, electrochromic structures are generally consisted of seven layers as; Surface / conductive thin film (TCO) / Electrolyte film / Ionic conductive layer / Opposite electrolyte film / Conductive thin film (TCO) / and Surface. Electrical conductor and optical transparent indium doped tin oxide (ITO) film that are of vital importance in electrochromic fiber structures, were deposited on the fiber surface along with the specially-designed magnetic sputter in order to coat the cylindrical surfaces within the scope of the thesis. Film deposition was repeated by replacing the ionizing gas (Ar) flow rate and the energy applied. While the structural characterization of thin films was carried out by means of optical microscope and scanning electron microscope (SEM), electrical characterization of deposited thin film, was carried out by a multi-meter (Ohm meter). In addition, the thickness of thin film that was magnified on the surface of the fiber, was calculated by SEM particularly, and also by different methods. As a result of the analyzes carried out, it was observed that ~ 40 sccm ionizing gas flow rate, 90 W applied energy, and 119 cm/min fiber feed rate increased the quality of the thin film acquired.

ÖZET

SİLİNDİRİK YÜZEYLERE İNDİYUM KALAY OKSİT (ITO) KAPLANMASI: ELEKTRİKSEL VE YAPISAL KARAKTERİZASYON

Keşfi yirminci yüzyılın ilk çeyreğine dayanan ve yarı iletken elementler sınıfına ait olan optik geçirgen iletken oksitler (TCOs), görünür bölgede (390- 700 nm) sergiledikleri yüksek optiksel geçirgenlik (≥ % 85) ve sahip oldukları düşük elektiriksek direnç (10^{-4} ohm.cm) sayesinde günümüz ve gelecek teknolojisinin yapı taşı olma niteliğindedir. Transistörlerden güneş panellerine, bükülebilir ekranlardan OLED lere kadar oldukça geniş bir uygulama alanına sahip olan optik geçirgen iletken oksitlerin en yaygın kullanım alanlarından biri de akıllı kıyafetler olarak bilinen tekstil malzemeleridir. TCO ların tekstil malzemelerinde kullanımı genel olarak renk değiştirme özelliğine sahip elektrokromik yapılar vasıtasıyla olmaktadır. Elektrokromik yapılar en genel anlamda 1.5 – 5 V luk düşük bir potansiyel fark altında indirgenme ve yükseltgenme reaksiyonları neticesinde sahip oldukları renkleri bir renk durumundan diğer bir renk durumuna geçiş ya da renksiz halden renkli duruma geçiş olarak değiştiren malzemeler olarak tanımlanabilmektedir. Her ne kadar uygulama alanına göre farklılık gösterse de en genel anlamıyla elektrokromik yapılar; Yüzey / İletken ince film (TCO) / Elektrolit film / İyonik iletken katman / Karşıt elektrolit film / İletken ince film (TCO) / Yüzey olarak yedi katmadan oluşmaktadır. Tez kapsamında elektorokromik fiber yapılarda hayati öneme sahip olan elektiriksel iletken ve optik geçirgen indiyum katkılı kalay oksit (ITO) film silindirik yüzeyleri kaplamak için özel olarak tasarlanılmış manyetik saçtırıcı ile fiber yüzeye kaplanmıştır. Film büyütme, iyonlaştırıcı gaz (Ar) akış hızının ve uygulanan güç miktarının değiştirilmesi ile tekrarlanmıştır. Elde edilen edilen ince filmlerin yapısal karakterizasyonu optik mikroskop ve taramalı elektron mikroskobu (SEM) vasıtasıyla yapılmış olup, büyütülen ince filmin elektiriksel karakterizasyonu multi metre (Ohm metre) kullanılarak yapılmıştır. Ayrıca lif yüzeyinde büyütülen ince filmin kalınlığı SEM görüntüleri başta olmak üzere çeşitli yöntemlerle hesaplanmıştır. Yapılan analizler neticesinde iyonlaştırıcı gaz akış hızının ~ 40 sccm, uygulanan güç miktarınının ~ 90 W ve lif ilerleme hızının 119 cm/dk olması elde edilen ince filmin niteliğini artırdığı görülmüştür.

Dedicated to;

My Family and Cem KAYA

TABLE OF CONTENTS

LIST OF FIGURES

LIST OF TABLES

CHAPTER 1

INTRODUCTION

1.1. Textile

Textile, derived from the Latin word ‘texere’ is defined, in the most general sense, as; to manufacture fabric by knitting or weaving yarns. The need for clothes, manufactured from textile materials, has arisen from the humankind’s need of protection against natural conditions. The production of petroleum-based synthetic fibers (nylon) in the midst of 20th century, in parallel with the high development of its technology, has gradually increased the significance of the relationship between textile industry and, technology. The integration of electronic devices; that are in solid form; onto the textile materials, can be accepted as the beginning of high technologic textile (Smart textile) application. This application has a wide area of use in various sectors, particularly in military industry and space research. Electronic devices integrated onto the textile structures; provide different opportunities such as; analyzing a user’s vital functions, finding a geographical position, and achieving a flow between the user and other electronic equipment (Detailed information is out of the scope of this thesis). Besides the integration of electronic devices onto the textile materials; especially the progress made in thin-film magnification techniques (Detailed information in chapter 2) concerning these structures that are called as smart clothes, has caused these structures to develop within the last few years, and to find a gradually increasing area of application. Antibacterial clothes (Taşdemir 2015), and textile structures that have thermal and electrical sensitivity, can be given as examples of these applications. In spite of the fact that the production of antibacterial textile material is made by magnifying the thin-film on the fiber that is directly used to weave the fabric (Özyüzer et al. 2010), other applications are performed only by the integration of the structure obtained, onto the textile material. The increase in the use of transparent conductive oxides (TCOs) in electronic industry (being applicable on flexible surfaces), along with the development of new deposition methods, provides new opportunities in terms of the application of high technology on textile materials.

The use of TCOs in textile materials, occurs by means of the electrochromic structures that generally have the feature of changing color.

1.2. Electrochromism

By massive increasing of interaction between man and machine, display devices has become an imperative for visual communication. The information which is to be communicated from a machine may usually be in the form of color images. Electrochromic displays device (ECDs) is one of the most powerful candidate for this purpose and it have numerus merits exempligratia multicolor, high contrast, optical memory, and no visual dependence on viewing angle (Monk, Mortimer, and Rosseinsky 2008). In the very most general sense electrochromism (EC) is known as the changing the color of the material under applying potential difference (1.5 - 5 V) (Granqvist 1995). An electroactive species often exhibits new optical absorption bands (i.e. shows a new colour) along with an electron transfer or 'redox' reaction in which it either gains or loses an electron. Redox reaction; chemical reaction involving reduction and oxidation simultaneusly. Fallowing relation may be ginven as an example of redox reaction.

$$[Fe^{II}(CN)_6]^{4-} \leftrightarrow [Fe^{III}(CN)_6]^{3-} + e^{-} \qquad (1.4)$$

(Pale) (Yellow)

Electrochromic materials are divided into three types as organics (Viologens, polymers), hybrids (Metallophtalocyanine, hexacyanometalates) and inorganics (Prussian blue, oxides, metal hybrids). There are only a few elements in the periodic table which have electrode behavior: Ti, Nb, Mb, Ta,W are demonstrate cathodic coloration, Fe,Co, Rh, Ni are demonstrate anodic coloration.

1.3. Transparent Conductive Oxides

Transparent conductive oxides (TCOs) are the semiconductor materials which have high optical transmission at visible wavelength (390 – 700 nm) and electrical conductivity close to that of metals (Ramanathan 2010). They also reflect near infrared and infrared (i.e., heat) wavelengths. This peculiar combination of physical properties is only achievable if a material has a sufficiently large energy band gap so that it is transparent to visible wavelengths, i.e., > ~3.0 eV, and also has a high enough carrier concentration, i.e., > ~10^{19} cm^{-3}, with a sufficiently large carrier mobility > ~1 $cm^2 V^{-1} s^{-1}$ that the material can be considered to be a 'good' conductor of electricity (Minami 2000). Although it has not been long time since the first TCO's were used in technology, the discovery of the materials dates back to first quarter of the twentieth century with the invention of transparent CdO thin film which was prepared by thermal oxidizing vacuum sputtered from cadmium metal in 1907 by Baedeker (Baedeker 1909). The three most common TCOs are In_2O_3, SnO_2, and ZnO, the basic properties of which are summarized in Table 1.1.

Table 1.1. The basic properties of the most conventional TCOs.
(Source: Wager 2003).

Material	Bandgap (eV)	Conductivity (S cm^{-1})	Electron Concentration (cm^{-3})	Mobility ($cm^2 V^{-1} s^{-1}$)
In_2O_3	3.75	10,000	> 10^{21}	35
SnO_2	3.35	8,000	> 10^{21}	20
ZnO	3.6	5,000	> 10^{20}	15

In the most general sense TCO materials in combination of different metals or metal combinations as form of $A_X B_Y$ (Where B is non-metal such as oxygen, A is metal or metal combination) or $K_z L_w M_p$ (Where M is non-metal, K and L metal or metal combination) as binary and ternary compounds respectively. In the table 1.2. The reader can see some examples of binary and ternary compounds.

Table 1.2. Binary and ternary transparent conductive oxides

Binary Compounds	In_2SnO_4	$CdSnO_3$	Zn_2SnO_4	$ZnSO_3$
Ternary Compounds	$Ga3_{-x}In_{5+x}Sn_2O_{16}$	$In_{1-x}Ga_{1+x}O_3(Zn)_k$ (k= 1,2,3)	$In_{4+x}Sn_{3-2x}Sb_xO_{12}$ (x=0-1.5)	$Zn_{2-x}Sn_{1-x}In_{2x}O_4$

In the beginning of this section transparent conductive oxides were determined as the materials, which have magnificent combination of the low electrical resistivity and high optical transparency. This characteristic behavior of TCOs mostly impossible in intrinsic stoichiometric oxides; nevertheless it may achieved both by producing them with a non-stoichiometric composition and introducing them with the feasible dopants (For instance; 1 Boron atom to 10^5 Silicon atoms). According to the dopant atom TCOs divided into two as n-type and p-type.

1.3.1. n - Type Transparent Conductive Oxides

If the majority charge carrier is electron in a semiconductor material, it is named as n-type transparent conductive oxide. AZO, In_2O_3 Sn (ITO), $ZnSnO_3$ and $Ga_{3-x}In_{5+x}Sn_2O_{16}$ may be given as examples. The carrier concentration of n-type transparent conductive oxides is around 10^{22} cm^{-3} which comes as a result of the resistance in the order of 10^{-5} And the band gap of these materials is approximately 3 eV with optical transparency in visible wavelengths about % 85 (Ginley, Hosono, and Paine 2010).

1.3.2. p – Type Transparent Conductive Oxides

With the difference of n-type, holes are the majority charge carrier in p-type TCO which results with the rising of the resistivity (Due to the large hole effective masses) (Hautier et al. 2013). The resistivity of this type oxides is in the order of 10^{-4} , the carrier concentration is about $10^{19} – 10^{21}$ cm^{-3} (Diesing, Hassel, and Lohrengel 1999) . The band gap of these kind material can be changed as worthy of note ($Cu_{1-x}B_xO_{2-\delta}$ has a bandgap

between 1.8 eV and 3.2 eV as boron content) with the optical transparency about %80 in the visible spectrum range (Tilley 2004). As well as n-type TCOs, p- type transparent conducting oxides also have binary and ternary compounds as $SrCu_2O_2$, $ZnRh_2O_4$, LaCuOSe (Scanlon 2011).

1.4. Organization of Thesis

The thesis is organized as follows; Chapter 2 introduces the theoretical background of the transparent conducting oxide. In chapter 2 it is also focused on the electrochromism in detail. In addition to those the deposition techniques of TCOs are given in the comprehensive form. Chapter 3 focuses on the experimental set-up (techniques) and characterization methods of this research. In chapter 4, the results and discussions are analyzed. The summary and the conclusion section are given later.

CHAPTER 2

TRANSPARENT CONDUCTIVE OXIDES AND DEPOSITION TECHNIQUES

2.1. Transparent Conductive Oxides (TCOs)

2.1.1. Transparent Conductive Oxides Basic

The discovery of the transparent conducting oxides (TCOs) dates back to the first quarter of the 20th century with the reporting of the CdO thin film which is prepared using thermally oxidizing vacuum sputtering (Facchetti and Marks 2010). The first application (Large scale) of TCOs was practiced in the period of World War 2. In following years TCOs have been employed in a board applications such as automobile, airplane and marine window, solar cell, electrochromic materials and touch screens. The extraordinary property of TCOs, which is combination of high optical transparency (~ 80 %) at visible spectrum range and high electrical conductivity, is achievable if and only if the material has adequately large energy band gap (~ 3 eV) with carrier concentration ~ 10^{19} cm^3. TCOs are nothing but semi-conductive materials, which have relatively high carrier concentration in the conduction band. The conductivity of TCOs is originated from both defects (Mostly Oxygen deficiency) and from extrinsic dopants. Pretty well all conventional TCO are n-type, in which majority charge carrier is electron. On the other hand p-type TCOs, where majority carrier is hole, are relatively new. The most in use TCOs are In_2O_3, Sn_2O_3, ZnO: Al, ZnO:Ga, Sn doped In_2O_3 (ITO) as binary, $Ga_2In_6Sn_2O_{16}$, $Zn_{2-x}Sn_{1-x}In_{2x}O_4$ as ternary. The reader is able to recognize composition space of most conventional TCOs in the figure 2.1

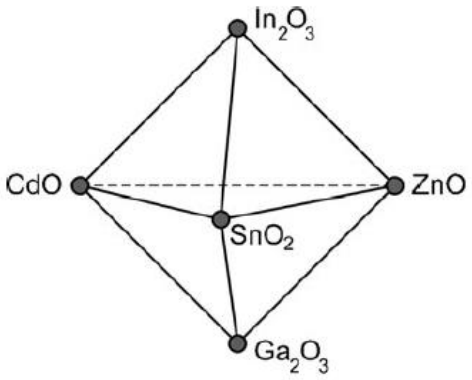

Figure 2.1. Composition space of most common TCOs
(Source: Ginley, Hosono, and Paine 2010).

The electrical resistivity of any TCO should be in the order of 10^{-5} with absorption coefficient, which is desired to be smaller than 10^4 cm^{-1} in the visible spectrum range and near UV. Indium doped tin oxide (ITO) is the TCO which is used in the scope of the thesis because of the properties it has such as low electrical resistance and high optical transparency (Tuna et al. 2010).

2.1.2. Electrical Properties of Transparent Conductive Oxides

TCOs known as the materials, which have electrical conductivity in the range of 10^{-2} -10^6 (S/m (SI)), that can be derived using Drudes free electron theory (Cohen 1998). This conductivity is a correlation of the number of charge carriers (Either holes or electrons). See the equation below.

$$\sigma = en\mu = \frac{1}{\rho} \tag{2.1}$$

Where σ is conductivity, ρ is resistivity, μ is mobility, e is the charge of the carrier, n is number of the charge carriers. With;

$$\mu = \frac{e\tau}{m^*} \tag{2.2}$$

Where m^* is the effective mass, τ is the relaxation time between collisions.

As it may be clearly understood from equations 2.1 and 2.2, in order to get higher conductivity either the number of the charge carriers or the mobility of charge carriers should be increased. Although increasing of the conductivity by doping (increasing the number of charge carries) has no negative effects directly, there occur some serious problems in the mobility of charge carriers, which is result of collisions between species in the material. Due to this reason the mobility of the charge carriers is limited as the number of charge carrier increase. The collisions known as scattering which can be written as the combination of different scattering mechanism as, lattice scattering, neutral impurity scattering, electron – impurity scattering, electron – electron scattering, ionized impurity scattering and grain boundary scattering (Scattering mechanisms are not included the scope of this thesis). If we reformulate equation 2.2;

$$\mu = \frac{e\tau}{m*} = \frac{e\lambda}{m* v} \tag{2.3}$$

Where v is drift velocity, λ is the mean free path. All of the parameters in equation 2.3 are effected by different scattering mechanism. Though total mobility may be written as:

$$\frac{1}{\mu_{total}} = \sum_i \frac{1}{\mu_i} \tag{2.4}$$

The reader can see the mobility and charge carrier density relation for some n-type semiconductors in the below figure.

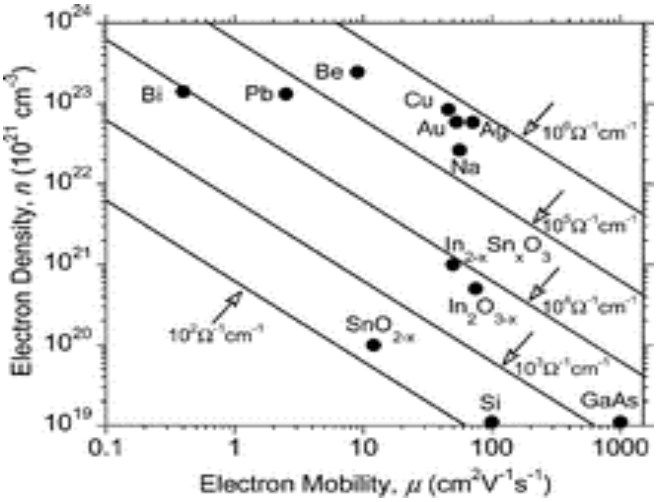

Figure 2.2. Relationship between mobility and carrier density of semiconductors. (Source: Slocombe et al. 2012)

2.1.3. Optical Properties of Transparent Conductive Oxides

Another important feature of TCOs is optical transparency at visible spectrum range (400 - 750 nm). This property is depends on the microstructure of the material, level of impurity atoms and growth techniques. Optical transmission may be defined using incoming light intensity and transmitted intensity.

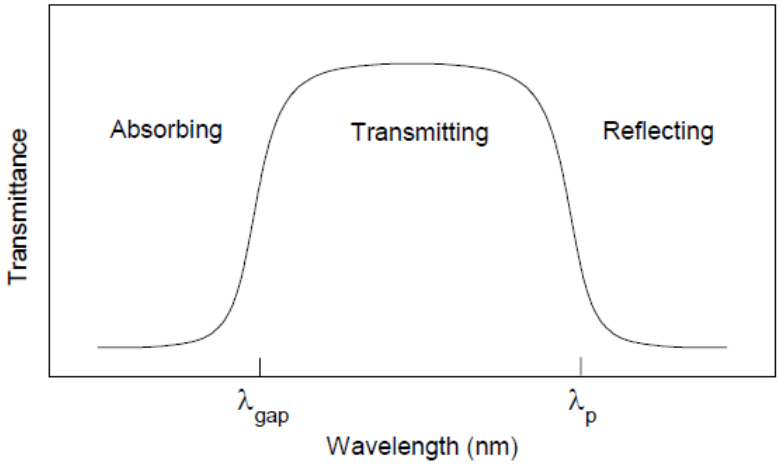

Figure 2.3. Spectral relation of TCOs. (Source: Vogelzang, Sikkens, and Sawatzky 1986)

Where λ_{gap} is the wavelength of band gap absorption, λ_p wavelength of free electron plasma absorption.

As it may be clearly noticed from the above figure, the transmission depends on the interactions between incoming light and material (TCO). This interaction may be determined using the oscillation (In Drudes model description free electrons would be thought as plasma and the plasma oscillate at a frequency, which is known plasma frequency.) motion of the electrons. For that reason let us rewrite the equation of motion of that electrons in the presence of time varying electric field (Photon is an electromagnetic field).

$$\frac{m\,d^2x}{dt^2} = \frac{-n_e e^2 x}{\varepsilon} \tag{2.5}$$

Where ε is the dielectric constant of TCO, n_e is the electron density and e is electron charge.

By solving this equation;

$$\omega_p = \sqrt{\frac{n_e e^2}{m\varepsilon}} \tag{2.6}$$

This frequency may be written using sputtering phenomenon (discussed in previous section) in terms of conductivity.

$$\frac{\sigma_e^0}{\varepsilon\tau} = \frac{n_e e \mu_e}{\varepsilon\tau} = \omega_p^2 \tag{2.7}$$

The refractive index may be determined as:

$$(n + ik)^2 = \frac{\varepsilon_L}{\varepsilon_0} - \frac{i\sigma}{\omega\varepsilon_0} = \langle N \rangle^2 \tag{2.8}$$

In the equation 2.8 the reader is able to recognize the reactive index is strongly depended on the frequency of the incoming photon. Furthermore the imaginary part component ‘k’ gives information about optical absorption.

$$\alpha = \frac{4k\pi}{\lambda} \tag{2.9}$$

Where α is absorption coefficient, k is excitation coefficient

2.1.4. Concluding Remarks

This section may be concluded by determining the correlation of optical properties and electrical properties. In order to do that, let us focus on equation 2.6

$$\omega_p = \sqrt{\frac{n_e e^2}{m\varepsilon}}$$

In that equation we can obviously recognize the plasma frequency is directly depends on the charge carrier concentration with the equation 2.1 on the other hand in equation 2.8 may be reformulate as;

$$N^2 = \varepsilon_{opt} - \frac{4\pi n e^2}{m^* \omega^2} \tag{2.10}$$

From equation 2.10 we are able to notice the refractive index depends on the carrier concentration as well. As a summary either electrical conductivity or optical transparency can be controlled by means of dopant atoms (donor or acceptor); the donor (acceptor) states change the electronic band structure of the material by introducing new carriers to the system. i.e., altering band structure has effects on the optical behavior of TCO directly and additional carriers alter the conductivity.

One should know; effective TCOs should represent both high electrical conductivity and high optical transparency at visible spectrum range simultaneously. This relation (or ratio) between conductivity and absorption coefficient known as the figure of merit (FOM) (Fang and Chang 2003). In the most general form FOM can be given as;

$$FOM = R_S\,[1 - T] = \frac{\alpha}{\sigma} \tag{2.11}$$

$$R_s = \frac{\rho}{d} \tag{2.12}$$

Where R_S is sheet resistance (which is the electrical resistance for thin film with uniform thickness d).

2.2. Electrochromism

2.2.1. Principle of Electrochromism

Electrochromism (EC) known as alteration of optical properties (Absorption, transmittance and reflectance) reversibly of a material when a voltage (1.5 - 5 V) is applied across it (Granqvist 1995). This phenomenon may be occurred if and only if a pertinent metal oxide (Transparent conductive oxide (TCO), which is going to be discussed in detail in the next section) is incorporated in the system. The voltage is applied across the material by means of this TCO's. See the figure below.

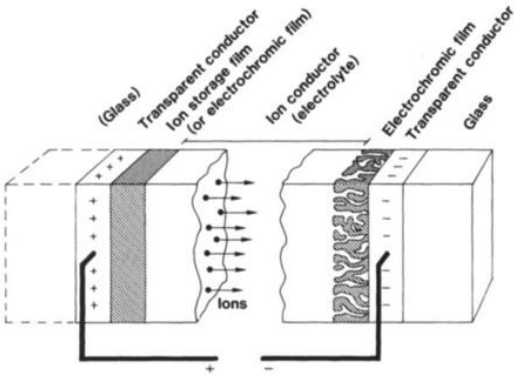

Figure 2.4.General structure of EC devices.
(Source: Granqvist 1995)

Typical electrochromic material consist of seven layers (See the figure above) by showing variations depending on the desired application: Substrate / TCO / Ion storage thin film / Ionic conductive layer / Electrochromic thin film (EC layer) / TCO / Substrate. Optical modulation of electrochromic layers (Ion storage layer and electrochromic layer) results from the oxidation and reduction reaction between them. The reader is able to notice some examples of these reactions below.

$$\frac{1}{2} Hg_2Cl_2(s) + e^- \leftrightarrow Hg(l) + Cl(aq) \quad (2.13)$$

$$[Fe^{II}(CN)_6]^{4-} \leftrightarrow [Fe^{III}(CN)_6]^{3-} + e^- \quad (2.14)$$

Electrochromic materials are divided into three types as organics (Viologens, polymers), hybrids (Metallophtalocyanine, Hexacyanometalates) and inorganics (Prussian blue, oxides, metal hybrids). In the figure 2.5 electrochromic oxides, which are in the periodic table, are represented

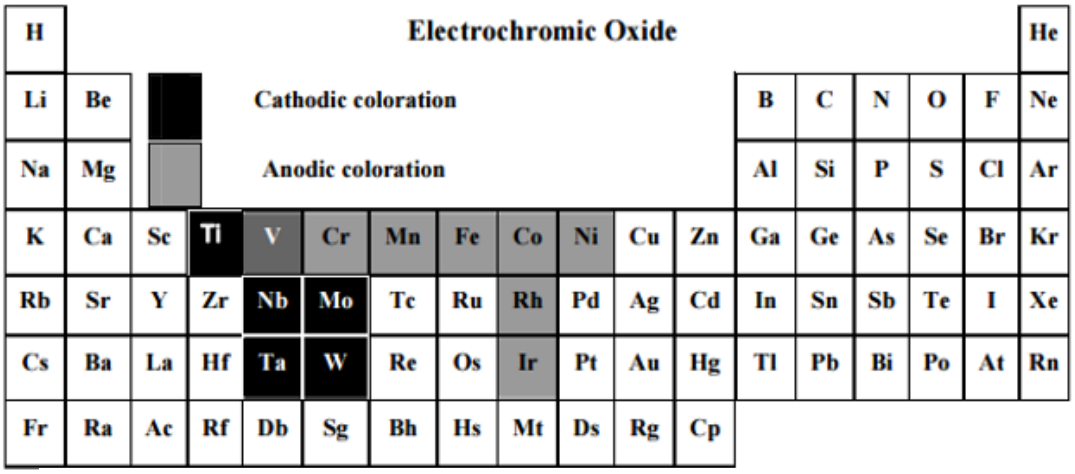

	Material	Color change	Full transparent
Cathodic	WO_3	Transparent ↔ Blue	Yes
	MoO_3	Transparent ↔ Blue	Yes
	Nb_2O_5	Transparent ↔ Pale blue	Yes
	TiO_2	Transparent ↔ Pale blue	Yes
Anodic	NiO	Transparent ↔ Dark brown	No
	IrO_2	Transparent ↔ Blue	Yes
	CoO_2	Red↔ Blue	No
	MnO_2	Yellow ↔ Brown	No
	PB	Transparent ↔ Blue	Yes
Cathodic & Anodic	V_2O_5	Pale blue ↔ Brown / Yellow	No

Figure 2.5. Electrochromic materials in the periodic table.
(Source: Monk, Mortimer, and Rosseinsky 2007)

To understand the working principle of this phenomenon, it is believed that focusing on the layers one by one is useful.

Electrochromic layer (EC): This layer shows both ionic conductivity and electron conduction simultaneously. There occurs a charge-balancing electron flow from TCO if ions are introduced from electrolyte (Core of the EC device). This electrons evoke a lasting change of optical properties. i.e. optical properties of materials (Elements) is controlled by changing electron numbers.

Ionic Conductive layer (Electrolyte): Can be either thin film or bulk form. This is also an electrical conductive structure in which free ions exists. One of the most important property of this layer is; high ionic conductivity (~10^{-6} S/cm) and low electron conductivity (~10^{-12} S/cm). Other important property is high optical transparency (>80 %).

Ion storage layer: This layer can show both electrochromic character or not, which supplies ions to the EC structure (Granqvist 1995).

Each of these layers has thickness less than one micron, which may be deposited by Chemical Vapor Deposition (CVD) and Physical Vapor Deposition (PVD), which are going to be discussed in detail in following sections.

There are some criteria for electrochromic devices as, higher coloration efficiency, low – switching time, high transmittance modulation, good memory effect and long cycle time which may be determined as follow:

Transmittance modulation (ΔT): Is depend on the change in the wavelength (λ)

$$\Delta T = T_b - T_c \tag{2.15}$$

Where T_b is balanced transmittance, T_a is colored transmittance. This modulation is about 75%

Coloration efficiency (CE): It is the magnitude of the optical modulation per injected / extract charge.

$$CE(\lambda) = \frac{\Delta OD\ (\lambda)}{Q} \tag{2.16}$$

$$\Delta OD\ (\lambda) = \log \frac{T_b}{T_c} \tag{2.17}$$

Where $\Delta OD\ (\lambda)$ is the optical density change, Q is charge density

$$Q = \frac{I\,t}{A} \tag{2.18}$$

Where I is current, t is time, A is area (cm^2)

Memory effect: Most important property of EC device. In the most general sense, retaining the color after removal voltage. The color may retain for hundreds of hours.

Cycle life: Depending on the application it may be ~5,000 cycle.

2.3. Transparent Conductive Oxides Deposition Techniques

2.3.1. Thin Film Growth Process

In the most general sense, thin film known as a thin (Less than one micron) layer of material onto a suitable substrate surface. Thin films are generally quasi-two dimensional structures which is widely used in many applications such as microelectronics, hard resistant coating, and optic.

Deposition process of the thin film can be sequenced as follows:

1- After impact to the substrate the unit species (ions, molecules or atom) lose their momentum component normal to the substrate, are physically adsorbed on the surface of substrate.

2- The species, which are absorbed from the surface, are not in the thermal equilibrium with the substrate surface, therefore they move (jump) on the surface. This movement causes an interaction between themselves resulting in formation as bigger cluster.

3- This step known as the chemical bond formation (chemisorption) between both cluster-cluster and cluster substrate. After reaching a critical cluster size the clusters become equilibrium thermodynamically.

4- The growth of the nuclei in number and size stops when the density of saturation is reached. The nucleation density of saturations (and size of the clusters) depends on the various parameters such as activation energy of adsorption, desorption and chemical structure of the surface. In that stage growth of the nucleus can be either perpendicular to the surface or parallel. Although there is a growth on both direction, lateral (Parallel to the surface) growth is dominant. In this stage the growth of the nuclei is named island.

5- After formation of the islands the coalescence starts, which is the result in the reducing of the surface area.

6- As a result of the integration of the islands, the thin film is formed on the surface.

See the figure below.

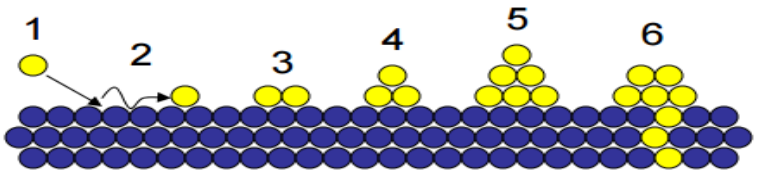

Figure 2.6. Formation of thin film.
(Source: http://users.wfu.edu/ucerkb/Nan242/L11-Thin_Film_Growth.pdf 2015)

Thin film is formed onto substrate as;
Frank-van der Merwe, Volmer - Weber, Stranski - Krastanov and reactive intermixing models. See the figure below.

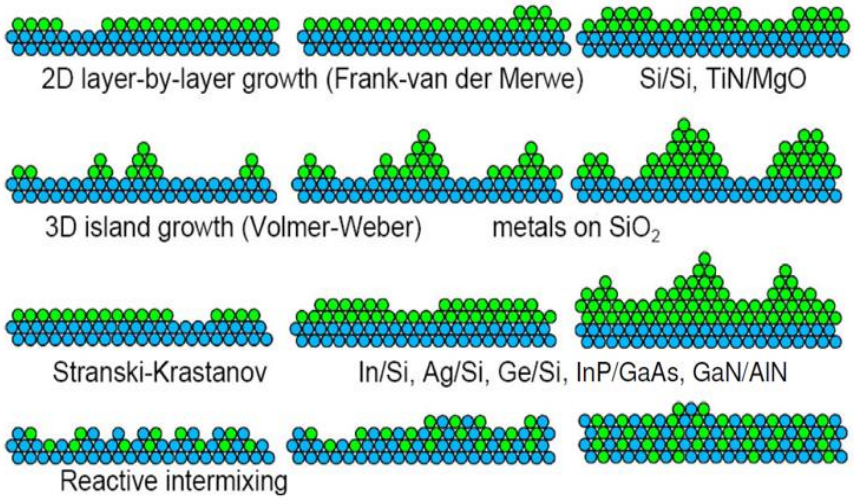

Figure 2.7. Formation types of thin film.
(Source: https://ece.uwaterloo.ca/~bcui/ Accessed august 13)

Deposition methods of thin film are divided into two fundamental categories as physical vapor deposition (PVD) and chemical vapor deposition (CVD). Although CVD technique is less expensive and time saving compared to PVD, it is not preferred in today's technology due to the low quality deposition. In the table 2.1 the reader is able to see the comparison of different thin film deposition techniques.

Table 2.1. Conventional thin film deposition techniques and their basic characteristic.
(Source: Wasa and Hayakewa 1992)

Process	Material	Uniformity	Impurity	Grain Size	Film Density	Deposition Rate	Substrate Temperature
Thermal Evaporation	Metal or low melting point materials	Poor	High	10~100 nm	Poor	1~ 20 A/s	50 ~ 100 °C
E-Beam Evaporation	Both metal and dielectrics	Poor	Low	10~100 nm	Poor	10~ 20 A/s	50 ~ 100 °C
Sputtering	Both metal and dielectrics	Very good	Low	~10 nm	Good	Metal:~ 100 A/s Dielectric:~1- 10 A/s	~ 200 °C
PECVD	Mainly dielectrics	good	Very low	10~100 nm	Good	10~ 100 A/s	200~300 °C
LPCVD	Mainly dielectrics	Very good	Very low	1~10 nm	Excellent	10~ 100 A/s	600~1200 °C

2.3.2. Chemical Vapor Deposition (CVD)

Chemical vapor deposition (CVD) is known as the deposition of a volatile compound of a material onto a heated substrate by means of a chemical reaction into a reactive gas enviroment. The deposition reaction may be created by various techniques suc as reduction, oxidation, compound formation or pyrolysis. The general structure of conventional CVD system is given in the figure 2.8.

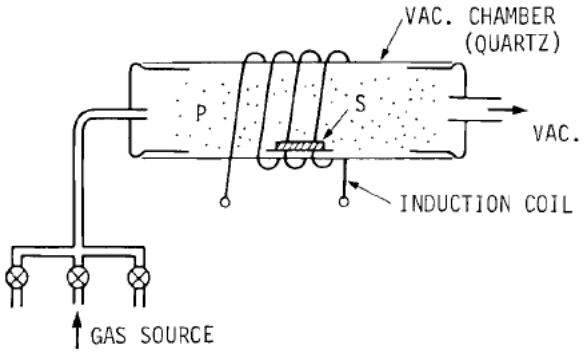

Figure 2.8. Chemical Vapor Deposition System.
(Source: Wasa and Hayakewa 1992)

In this technique deposition rate in a range of 100 to 1000 A^{o}/min and it varies exponentially with the increasing substrate temperature (For most application; substrate temperature is at the range of 600 to 1000 ^{o}C) and the operation pressure is about 1 mtorr, which is very low if it is compared to physical vapor deposition technique, even it is possible operate in atmospheric pressure. The operation process of every CVD technique may be sequenced as follows:

1- Convection of the reactance (Precursor) gases into the reaction region.
2- Gas phase reaction in order to produce different reactive agents as well as by-products.
3- Transportation of the reactance and newly produced agents onto the substrate
4- Chemical and physical absorption and decomposition reaction of these species on the surface.
5- Deposition on the substrate.
6- Desorption of the evaporative by-products.
7- Transportation of the by-products from reaction region.

As it may be clearly understood from the sequenced, the method based on some complicated principles such as chemical kinetics and fluid mechanics for that reason it is not possible to go in more detail according to the scope of this thesis.

Requirement of the high efficiency of chemical reactions and request of variations on both substrate and deposited material lead an improvement to the technology as a result of this various CVD techniques have been developed such as low pressure CVD (LPCVD), metal organic CVD (MOCVD) and Plasma - assist CVD (PACVD). Among all these techniques PACVD becomes a prominent because some advantages such as high energetic particles, improved reaction efficiency and high adsorption and deposition rate. See the figure below.

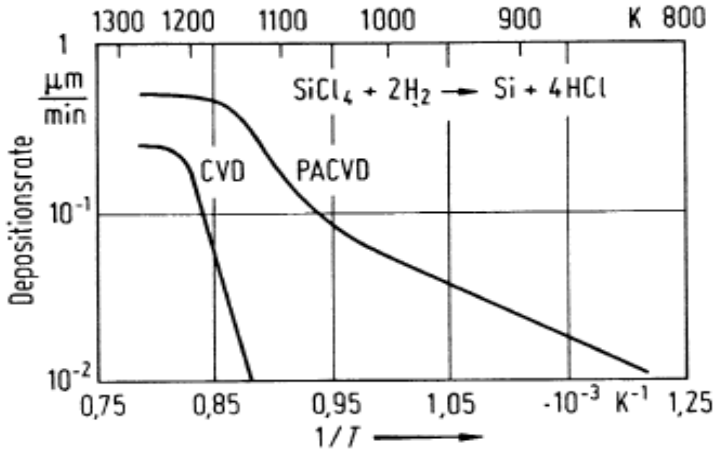

Figure 2.9. The basic comparison of CVD and PACVD
(Source:http://static.ifp.tuwien.ac.at/homepages/Personen/duenne_schichten/pdf /t_p_ds_chapter2.pdf 2015).

2.3.2.1. Plasma-Assisted CVD (PACVD)

Plasma- assisted CVD is nothing but the modification of traditional CVD. In this technique a plasma, which is rf induced, is used to gained extra energy to reactant gases in order to run the process at lower temperatures (~ 300 ^{o}C). Due to controllability of the substrate temperature by cooling mechanism, the surface reaction is limited. Figure 2. 10 is represents a basic PACVD system.

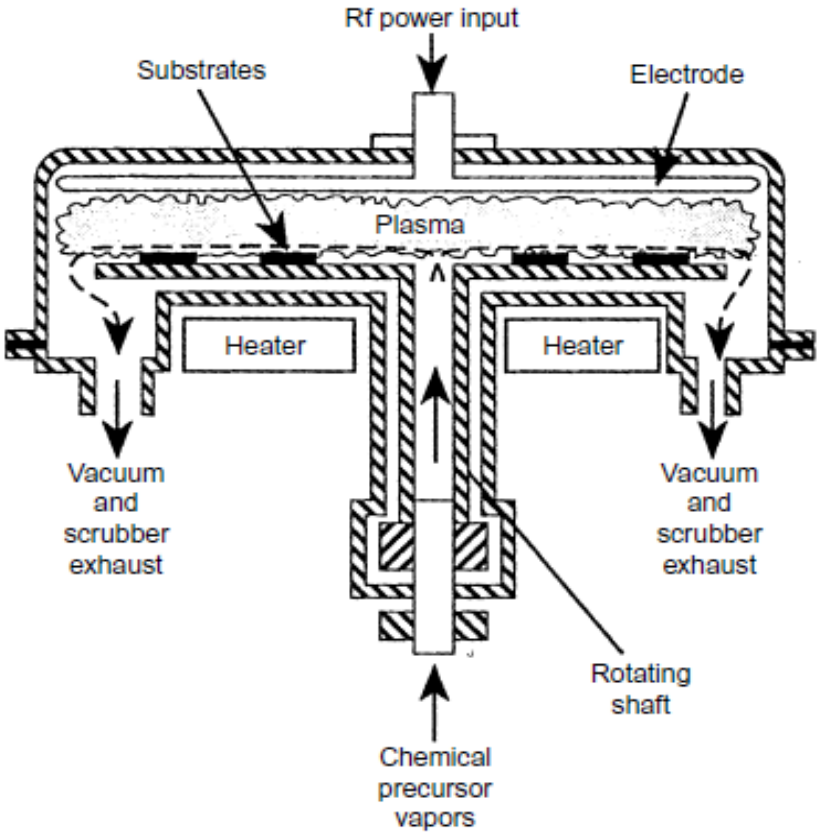

Figure 2.10. Parallel plate plasma assist chemical vapor deposition system (Source: Mattox 2010).

In this technique working pressure is between 0.1 and 1.0 torr, which results in lower mean free path. The ionization is in the order of 10^{-4}, as a result of this, the gas molecules in the reactor is mostly in neutral form. The electrons in the reaction region gain energy (as well as ions) from the electric field in that region and typical electron energy is ~ 6 eV, which means the temperature of electron is 50,000 K. (Wasa and Hayakewa 1992). The electrons, which have gained high energy, increase the chemical reaction in the plasma resulting in the reduction of the temperature of reaction.

2.3.3. Physical Vapor Deposition (PVD)

Physical vapor deposition (PVD) is known the atomic or molecular size deposition technique where material is vaporized from mostly a solid target in the form of atoms (molecules) and transported in the form of a vapor by the medium of a low pressure gaseous or plasma environment to the substrate, in which they condense. PVD technique is preffered for thin film deposition due to many advantages it has, suc as; film uniformity, thickness accuracy, and process repeatability. In the most general sense physical vapor deposition (PVD) technique can be determined with three basic sequence steps;

a) The material (target) to be deposited is physically converted into vapour phase from solid state.

b) The vapour is transported across a region of reduced pressure from the target to the substrate.

c) The vapour condenses on the substrate to form the thin film.

The reader is able to see fundamental pysical vapour deposition techniques in pictorial form in the following figure.

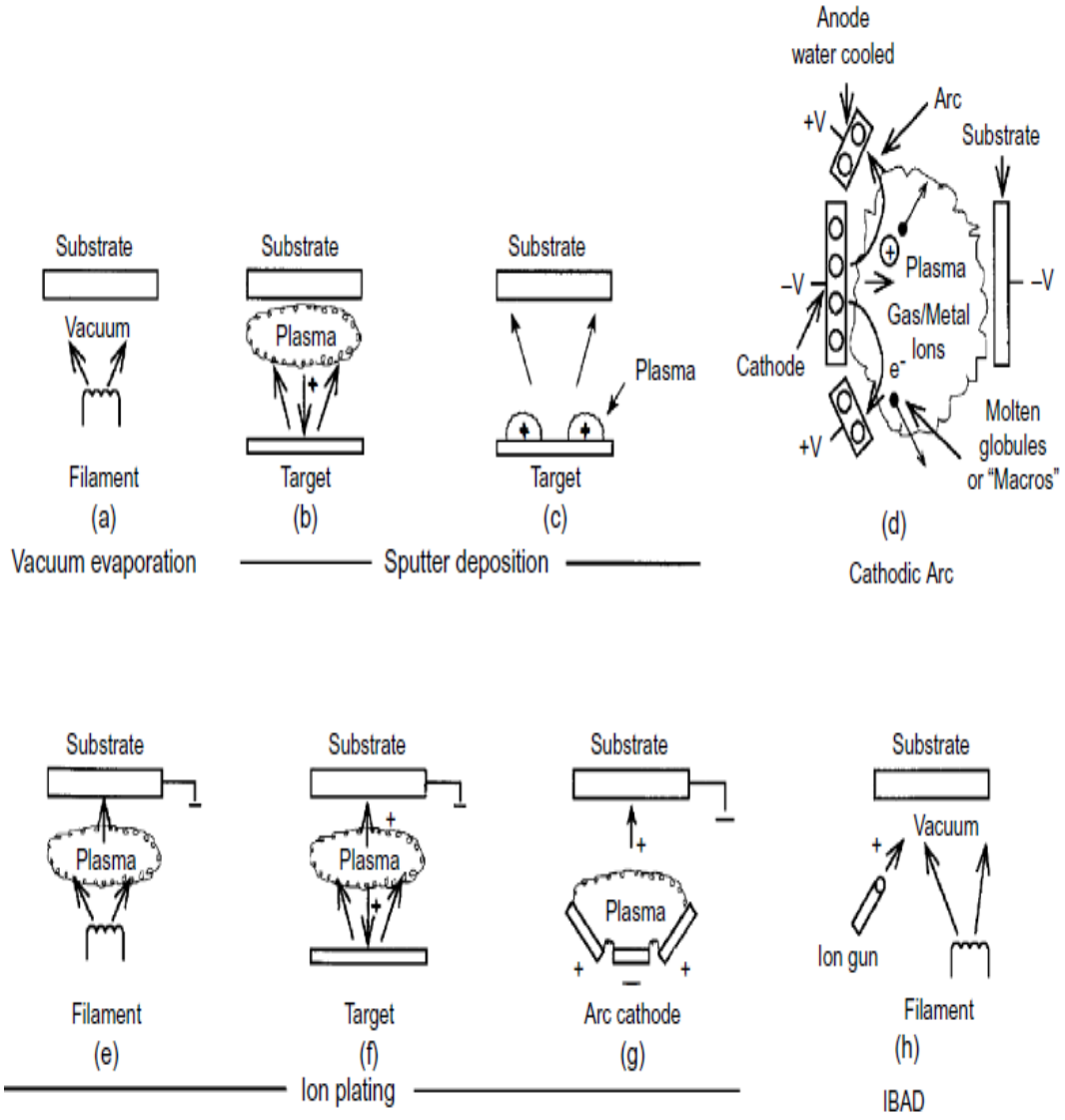

Figure 2.11. Fundamental PVD techniques
(Source: Mattox 2010).

The deposition rate depends on the vacuum chamber pressure, target to substrate distance and substrate temperature. Vacuum camber pressure (P) has significiant effects on the quality of the film since it is directly related to the mean free path (The lower pressure results in the higher mean free path (λ)). The fundamental realation between those quantities are given in the fallowing equation.

$$P \sim 1 / \lambda \tag{2.19}$$

In order to get the thin film of high purity and good quality, the pressure should be low ($\approx 10^{-3} - 10^{-4}$ torr) The quality of the vacuum is very significative and an useful consideration in determining the deposition rate, since impurity atoms in the deposition chamber may impinge on the growing film resulted in a non-stiochiomctirc film. Therefore, complete evacuation of a deposition chamber with optimizing growth parameters may lead to high quality of thin films. Beside the minimization of the base pressure (the presure of the chamber before deposition), types of substrate are important as well. Substrates can be divided into three types: metal, semiconducting and insulating materials that have their own advantages. PVD techniques are used to deposit films with thicknesses at the range of a few nanometers to thousands of nanometers even milimeter according to the desired application (Wasa and Hayakewa 1992). An other importand advantage of PDV thecnique is the selection of deposited materials : Metals, alloys, semiconductors, metal oxides, carbides, nitrides, cermets, sulfides ect.

To go into further details, branching the PVD techniques into two category is going to be useful as evaporation technique and sputtering technigue. Altough there are much more PVD techniques, only the most importand ones are discussed with in the scope of this thesis.

2.3.3.1. Evaporation

Despite the fact that evaporation is known as the oldest thin film deposition technique requires relatively high vacuum, it is still widely used for depositing thin films. This technique may be used for a very large number of materials including metals and metal alloys even it is possible to deposit some of the low-molecular weight polymeric materials (Mattox 2010). The processes of evaporation; resistive or electron beam heating is applied to the target in order to make the deposition material evaporate. The evaporated atoms are thermalized and have a kinetic energy of 0.025 eV (in other words they have gained momentum) after evaporation the deposition atoms are transport from target to substrate and the vapor condenses on to the substrate as final phase (Fuller 2011). In the figure 2.12 e-beam and resistance heating evaporations can be seen.

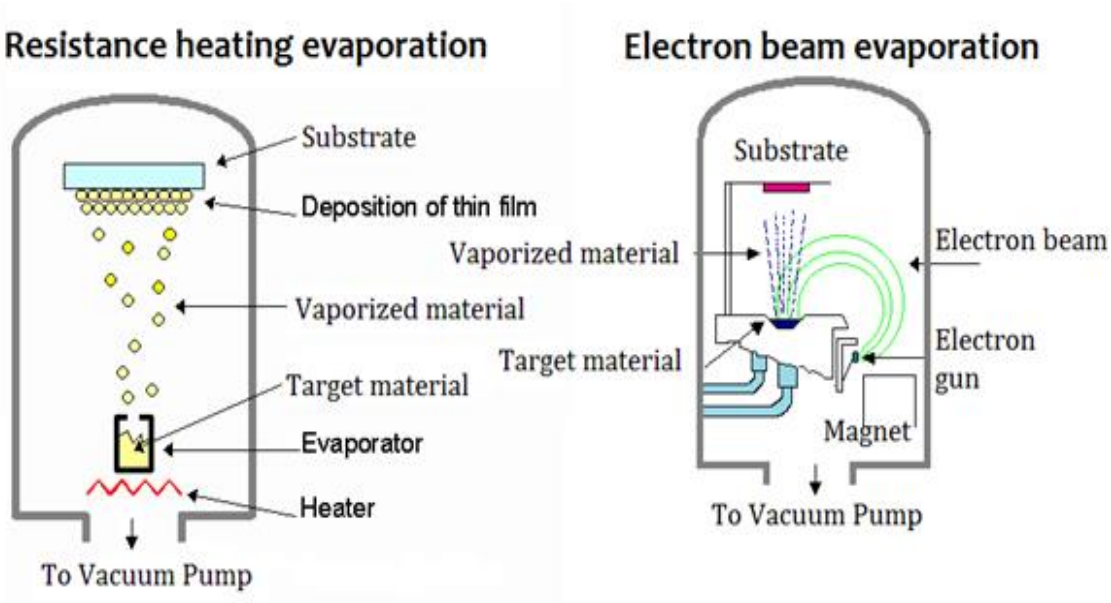

Figure 2.12. Thermal evopatarion thecniques.

The properties of the film are depend on some basic quantities such as pressure of the chamber, distance between evaporation source and substrate and impurity atoms in the chamber. In the most general sense the evaporated atoms should cover a distance between evaporation source to substrate hence collisions between evaporated atoms and impurity atoms must be as small as they can be. This requsite introduce us to some paremeters such as mean free path, arrival ratio and deposition rate.

Vaccum pressure of the chamber has significiant effects on those quantities espacially on the mean free path (distance between two collisions) of the evaporated particle. See the equation below.

$$\lambda = \left(\frac{n}{V} \pi \sigma^2 \sqrt{2} \right)^{-1} = \frac{kT}{\sqrt{2}\,\pi\,\sigma^2\,P} \qquad (2.20)$$

Where λ is mean free path, n is number of the patricle, V is the moving speed of the particle, σ is the radius of the particle, k is the Boltzman constant, T is the temperature, P is the pressure of the vacuum chamber. For example if λ is 30 cm the requried pressure is 2.6 x 10^{-4} torr. We might find out that each materials has different mean free path in the eguation 2.20 an other importand quantitiy is Arrival rate, which is known as the number of film molecules hitting the surface per second is the same as the number of gas molecules. In the tabl 2.2 the relation between pressure vs arrival rate is given.

Table 2.2. Arrival rate vs pressure.

Pressure (Torr)	Mean free path	Arrival rate
10^{-1}	0.5 mm	10^{-4}
10^{-3}	5 cm	10^{-2}
10^{-5}	5 m	1

For materials which is very reactive with the gas as Ti or O_2, the film can be very impure when arrival rate is very close to one.

The most important quantity of the evaporation technique is the deposition rate beyond any doubt. Deposition rate exhibit different characteristic according to the selected source (both point source and planar source) material. See the figure below.

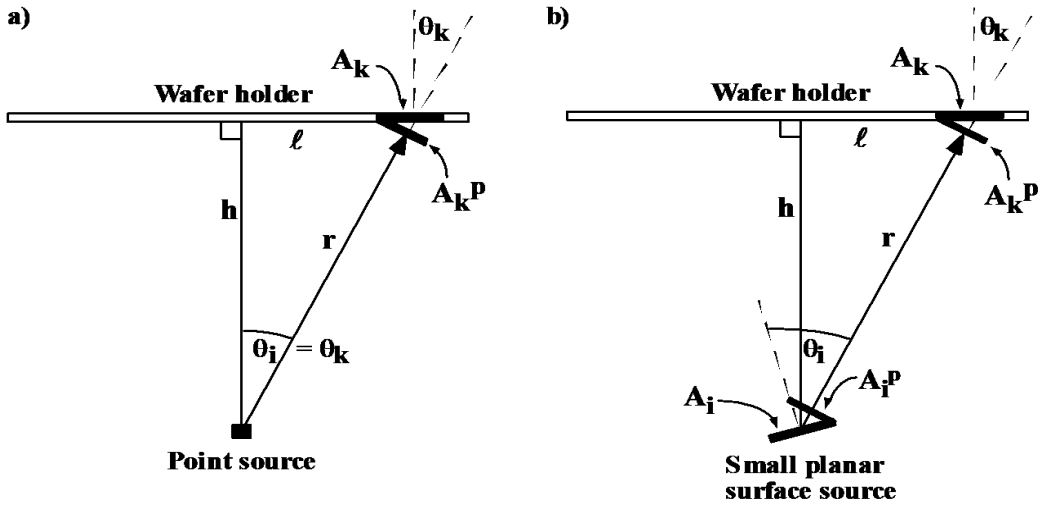

Figure 2.13. a) Point source evaporation mechanism, b) Small planar source evaporation mechanism

For point source;

$$F_K^P = \frac{R_{evap}}{\Omega r^2} \tag{2.21}$$

$$V = \frac{R_{evap}}{\Omega N r^2} \cos\Theta_k \tag{2.22}$$

For planar source;

$$F_K^P = \frac{R_{evap}}{\pi r^2} cos^n \Theta_i \tag{2.23}$$

$$V = \frac{R_{evap}}{N\pi r^2} cos^n \Theta_i \cos\Theta_k \tag{2.24}$$

Where;

F_k: The outward Flux, V: Deposition rate (nm/sec), N: Density of the evaporated material

R_{evp}: Evaporation rate from the source, Ω: Solid angle; 4π if source emits in all directions, 2π if the emitting is only in one direction.

In the figure 2. 14 the deposition rates of different materials are given.

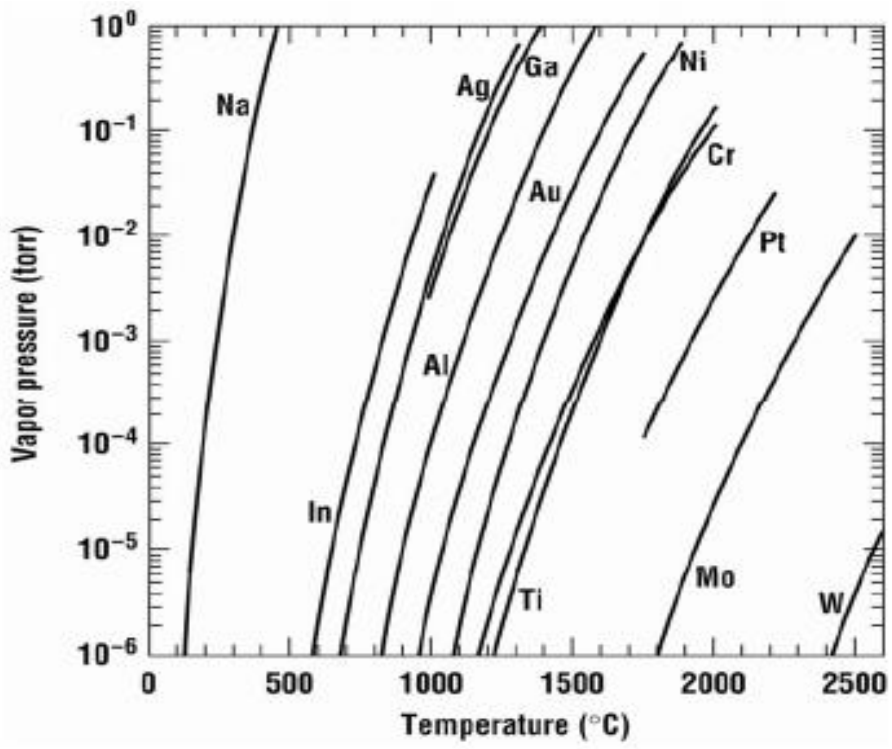

Figure 2. 14. Deposition rate vs source temperature
(Source: Boone 1986).

Typically deposition rate: ~ 0.5 μm / min (~ 8 nm / s) for Al.

2.3.3.1.1. Resistive Evaporation

Physical vapor deposition technique, which requires relatively high vacuum level introduced to the thin film technology with resistive evaporation technique. This technique comprises evaporating source materials in a chamber (which has vacuum level about 10^{-6} torr) and condensing the evaporated particles on a substrate. In a detailed form: The material is heated until fusion by means of an electrical current passing through a filament or metal plate, in which the target material (evaporation source) is deposited. The evaporated material is then condensed on the substrate. In this technique the electrical current, which passes through evaporation source causes the heating of the material due to the material's resistance. Each deposited material needs different evaporation source. In the figure 2.15 the types of evaporation sources can be seen.

Figure 2.15. Evaporation sources.

See some materials and evaporation sources with basic information in the table below.

Table 2.3. Materials with their proper thermal sources

Material	Melting Point (°C)	density g/cm3 at 20°C	Temp.(°C) for Given Vap. Press. (mBar)			Thermal Sources			
			10^{-8}	10^{-6}	10^{-4}	Boat	Cubic	Basket	Crucible
Zn	420	7.14	-	-	~ 2000	W, Mo	W	W	Al_2O_3
V	1890	5.96	1162	1332	1547	Mo	-	-	-
WO_3	1473	7.16	-	-	980	W, Pt	-	-	-
SnO_2	1630	6.95	-	-	~ 1000	W	W	W	Al_2O_3
Ag	962	10.5	574	685	832	W	Mo	Ta, Mo	Al_2O_3

2.3.3.1.2. e-Beam Evaporation

In this evaporation technique an intense beam (e-beam) energy is applied locally to the evaporation source instead of the resistive heating. The electrons, which are removed from the filament, are directed to the target via magnets. See figure 2.12. Desired voltage is about 5 kW to dismantle the electrons. This evaporation method has a pore ability just like thermal evaporation when covering the steps, which also makes this method ideal for lift-off processes. One of the remarkable advantage of e-beam evaporation over resistive evaporation is the possibility to inset a larger amount of energy into the evaporation source. Which yields a higher density thin film with an increased adhesion to the substrate (Moshfegh et al. 2004). As the electron beam only heats the source material and not the entire basket, a lower degree of contamination from the basket will occur compared to the case of thermal evaporation. By using a multiple basket e-beam gun, several different materials can be deposited without breaking the vacuum. In the table 2.4 some materials are given with their basic evaporation properties.

Table 2.4. Chosen materials with basic properties and their suitable evaporation sources

Material	Melting Point (°C)	density g/cm3 at 20°C	Temp.(°C) for Given Vap. Press. (mBar)			E-Beam	
			10^{-8}	10^{-6}	10^{-4}	Suitability	liner
Al	660	2.70	677	807	972	Ex	Gr, Int
Cu_2O	1235	6.0	-	-	~600	G	Al_2O_3
In	157	7.30	487	597	742	Ex	Gr, Mo, Al_2O_3
MoO_3	795	4.69	-	-	~900	-	Mo, Al_2O_3
Ti	1660	4.5	1067	1235	1453	Ex	Gr

2.3.3.2. Sputtering

Sputtering is widely used technique for depositing thin film. And mostly practiced by means of plasmas.

Plasmas; is the ionization of any gasses (mostly Ar^+, Kr^+) by the medium of electric field.

In the most general sense, sputtering is the continuum of etching of that surface of the target material with high energetics ions. Sputter deposition is nothing more than the assembly of the sputtered atoms (etched atoms) onto a substrate which is close (distance between target and substrate at a range from ~ 50 to ~ 150 mm) to the target material (Seshan 2012) .

If it is compared to the evaporation technique, sputtering has many advantages such as high adsorption coefficient, more homogeneity of thin film and much more target material choice (almost unlimited). Before begining to describe the physics behind of the sputtering process, a basic understanding of the ion-surface interaction is requried. The interaction between target atoms and ions is mainly depend on mass of the ions (Ar^+, Kr^+) incident energy, which means a minimum enegy (threshold energy) is required to sputter and the crystal structure of the substrate. See the folowing ionization process.

$$Ar + e^- \rightarrow Ar^+ + e^- + e^- \quad (2.25)$$

$$Kr + e^- \rightarrow Kr^+ + e^- + e^- \quad (2.26)$$

The interaction between ion and target is represented according to the energy range in the figure 2.16 as it was seen in the figure, sputtering occures between 10^2 and 10^4 eV (it depends on the vacuum level of the sputtering chamber).

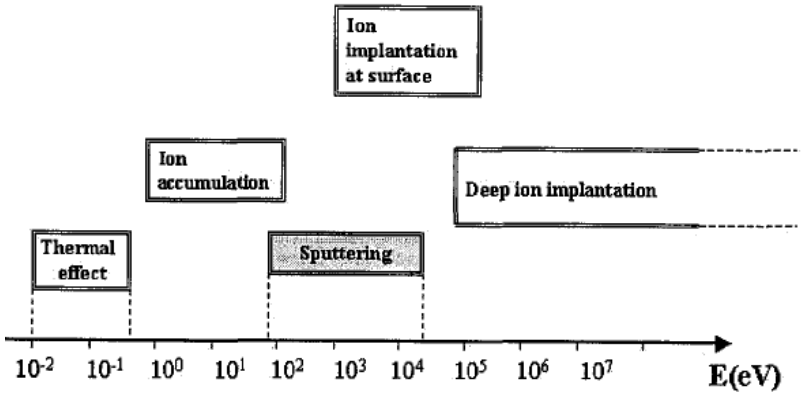

Figure 2.16. Ion-surface interaction with their energy range.
(Source: Moshfegh, Kanel, and Kashyap 2004)

Phenomenon in the sputtering technique is the physical momentum and kinetic energy transfer between energetic atomic-sized particles (ions) and the atoms of the target (solid cathode) material and this is not depend of the charge of the particle. By the interchanging of momentum and kinetic energy, many effects might be produced on the collisions such as elastic or inelastic; in the first type of collision, mainly reflected particles may be found. In the second type, the collisions may introduce secondary electrons, photons, X-ray and implanted particles. The interactions between charged particles and the target material are represented in the figure 2.17.

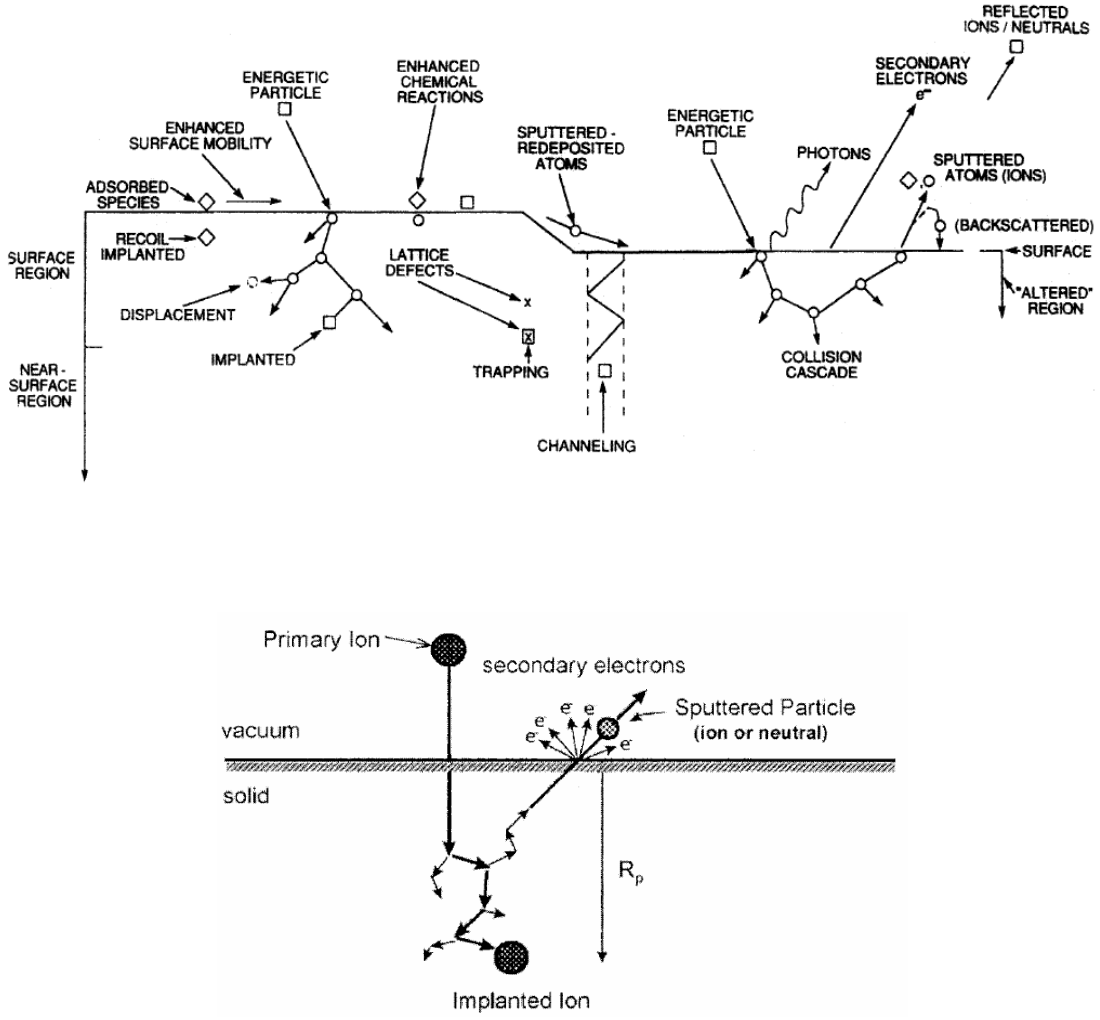

Figure 2.17. Schematic diagram of the sputtering process and ion-solid interactions (Source: Mattox 2010, Prenitzer 2000).

Where R_p is the covered distance in the solid by ion.

The interaction between ion and target might be detailed as follows:

1- Ions, which bombard to target material, would be originated from either plasma or ion beams.

2- The collision between ions and target material may result in:

The ions can reflect back, stick on the surface, eject or sputter surface atoms or can be absorbed from material and get buried in the target (ion implantation).

NOTE:

Ion beam/ion energy is crucial when determining the interaction; if the ions' energy is about 10^{-2} eV, it means they stick on to the target. At higher energies ions might penetrate into a quite deep point of the target, which results in reduction of the sputtered atoms (Moshfegh et al. 2004). Hence the ions should have proper energy level to etch the atoms from surface of the target. In the figure 2.18 the sticking probability of particle is given with respect to the energy.

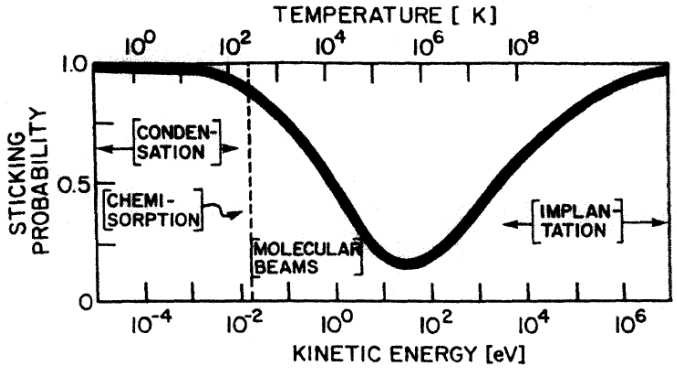

Figure 2.18. Particle sticking probability as a function of energy

(Source: http://www.physik.uni-wuerzburg.de/EP4/teaching/WS2007_08/technikseminar/InsituPreparationws0708.pdf Accessed).

As it is clearly noticed, the sticking probability reaches its minimum of 0.2 at 20 eV.

3- As a result of ion bombardment, diversely charged particles (e.g.,electrons, ions), neutrals, and photons of varying energies and abundances are emitted from the surface.

There are three regimes of sputtering (according to the ion energy) in the litrature, which are symatically depicted in the figure 2.19. Because of detailed information of this phenemonon is out of the scope of this thesiss, the first two are only given inthe basic form.

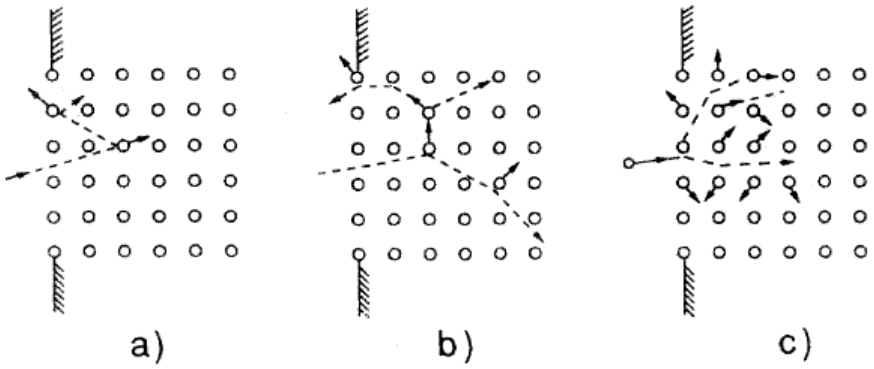

Figure 2.19. The Energy regimes of sputtering, (a) very low energies, (b) linear cascade (Source: Ohring 2001)

a- Very low energies (Single knock – on); Incident ion energies a few eV or so up to 30–50 eV, there is little sputtering occur.
b- Linear cascade; Incident energies between 40 and ~1000 eV, the energetics ion has more than enough energy and momentum to dislodge large amount of atoms (Ohring 2001).

Sputter yield:

Sputter Yield (S), which is defined as the mean number of sputtered target atoms per incident ion that is a measure efficiency of sputtering. See the equation below.

$$S = \frac{\text{Number of sputtered atoms}}{\text{Incident particle}} = \alpha \frac{Mm}{(M+m)^2} \frac{E_m}{U_M} \qquad (2.27)$$

Where M is mass of target atom, m is mass of ion, E_m is kinetic energy of ion, U_M is bonding energy of target atom, α is depends on striking/incident angle.

It might be also measured by various methods such as weight loos of the target, dedection of sputtered particle in fllight. Experiments show us sputter yield in a range from 10^{-5} to 10^{3} (Malherbe and Odendaal 1999). Figure 2. 20 represents the sputter yield with respect to the ion energies for most preferred materials.

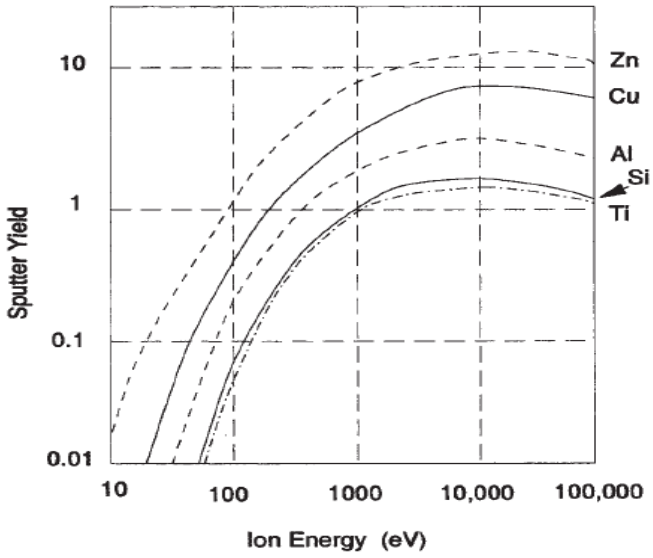

Figure 2.20. Sputter yield of conventional elements as a function of ion energy (Source: Seshan 2012).

There is a direct correlation between sputter yield and ion energy as it could be recognized from the figure 2.20, See the equation below. Threshold energy (E_0); is the minimum energy required to remove a target atom from the surface. For conventional elements; 15 eV < E_0 > 40 eV (Moshfegh, Kanel, and Kashyap 2004).

$$E_{threshold} = \frac{Heat\ of\ Vaporization}{\gamma(1-\gamma)} \tag{2.28}$$

$$\gamma = \frac{4mM}{(M+m)^2} \tag{2.29}$$

In addition to the energy of the ion sputter yield also depends on the angle of the collision (Yamamura, Itikawa, and Itoh 1983). Following equation represents the relation between sputter yield and incident ion angle.

$$S(\eta) = \frac{S(0)}{\cos\eta}\ e^{[f\ x\ \cos\gamma\ x\ (1-\frac{1}{\cos\eta})]} \tag{2.30}$$

Where S(0) is the sputter yield at 0^o angle to normal of the substrate, γ is optimum angle of incidence for maximum sputter yield. Here f may given as

$$f = \sqrt{E_b}\ x\ [0.94\ -\ 1.33\ x\ 10^{-3} x \frac{m_r}{m_p}] \tag{2.31}$$

Where E_b is binding energy of target atoms, m_r is sputterd atom mass, m_p is the mass of the ion (Moshfegh et al. 2004).

The sputter yield approaches saturation for higher energies (ex: Xe^+ ~100 keV and Ar^+ ~20 keV) (Moshfegh, Kanel, and Kashyap 2004). Sometimes, at very extreme energy levels, the yield in a decrease fashion because of the increasing penetration depth and hence increasing energy loss below the surface (This is why sputtering process is known as a surface phenomenon), i.e. not all the affected atoms are able to reach the surface to escape. In the table 2. 22 Sputter yields for commonly used materials (Ion: Ar^+) are listed.

Table 2.5. Sputter yields of most preferred materials as a function of ion (Ar^+) energy (Source: Seshan 2012).

Element	300 eV	500 eV	1000 eV
Ag	1.7	2.5	3.5
Al	0.6	0.9	1.5
Mo	0.3	0.5	0.9
Si	0.3	0.7	1
Sn	0.6	0.9	1.4
W	0.3	0.5	0.9
Zn	3.7	5	7

Another important quantity is sputter rate, which may occur by using sputter yield. See the following equation.

$$Я = \frac{S(E_i)\, J_i}{\rho e} \frac{M}{N_A} \; [ms^{-1}] \qquad (2.32)$$

Where, $Я$ is the sputter rate, S is the sputter yield, E_i is ion energy, M is molar mass of the target, ρ is target density, J_i is ion current, eN_A is 9.649 x 10^7 [Askmol^{-1}].

The emission process of sputtered atoms differ from evaporation technique due to their kinetics. Sputtered atoms peaks at about 5 eV than decreases as $1/E^2$. In general sense, kinetic energy of sputtered atom much higher than the kinetic energy of evaporated atoms (Seshan 2012). See the figure below.

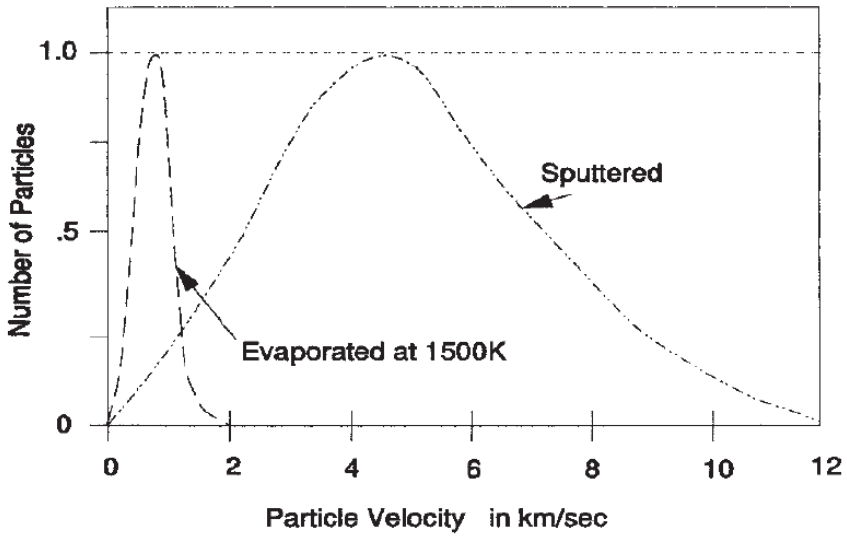

Figure 2.21. Kinetic energy distribution for sputtered Cu vs evaporated Cu (Source: Seshan 2012).

Unlike evaporated atoms, sputtered atoms track a cosine distribution. See the figure below.

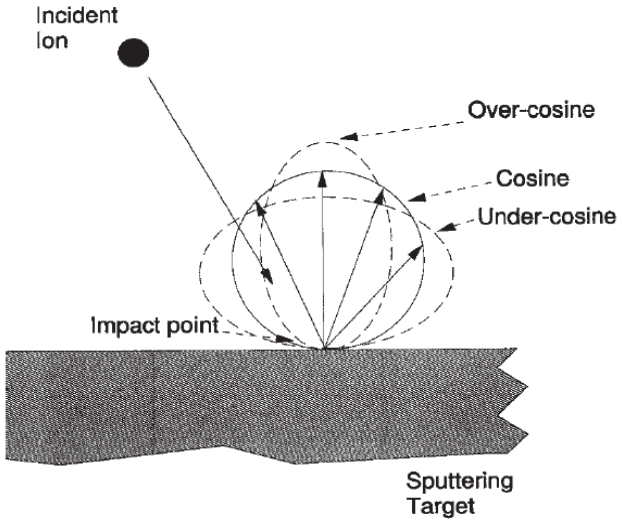

Figure 2.22. Sputter distribution of Cu atoms (ion: Ar^{+}) (Source: Seshan 2012).

According to the energy of the ion, the geometry of the sputtered atom distribution exhibits an alteration; if the ion energy is increased the emission becomes more peaked, which is corresponds to over-cosine. If the ion's energy reduces, the emission becomes lower peaked which is named as under-cosine (Seshan 2012).

Thus far it was only discussed the interaction between target atoms and ions videlicet the mechanism of sputtering. At this juncture it is necessary to go into further detail how the ions (Plasma) generated. Amongst all sputtering techniques in the literature, the simplest one is the diode (DC and RF) sputtering. DC diode sputtering mostly preferred to deposition conductive materials but to deposition dielectric materials RF (radio frequency) power supply is needed. See table 2 .6

Table 2.6. Some conventional materials and deposition techniques.

Material	Melting Point (°C)	density g/cm3 at 20°C	Temp.(°C) for Given Vap. Press. (mBar)			Sputter
			10^{-8}	10^{-6}	10^{-4}	
In_2O	~ 600	6.99	-	-	~ 650	RF
MoO_3	795	4.69	-	-	~ 900	RF
Si	1410	2.32	992	1147	1337	DC, RF
VO_2	690	3.36	-	-	~ 500	DC, RF
ZnO	1700	3.98	-	-	~1800	RF
WO_3	1473	7.16	-	-	980	RF

In the most general sense diode sputtering system is composed of a pair of electrodes. One of the electrodes is cold cathode (usually target) and the other is anode (usually substrate). See the figure below.

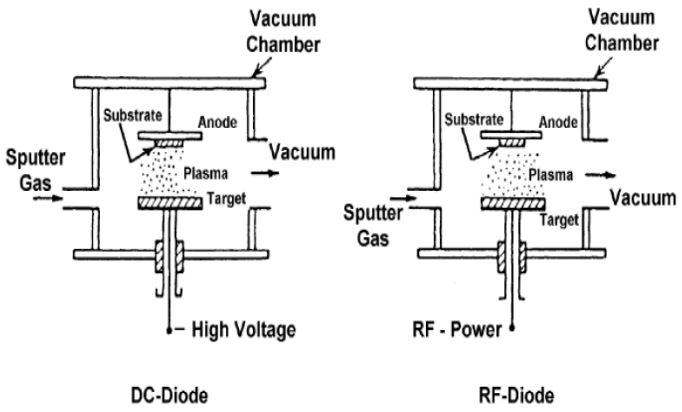

Figure 2.23. DC and RF sputtering systems.
(Source: Wasa and Hayakewa 1992)

2.3.3.2.1. DC Sputtering

If high DC voltage (typically 2 – 5 kV) is applied between a pair of electrode in a gaseous atmosphere (mostly Ar^+), that will result in the ionization of the gases. See the following ionization process of Ar gas.

$$Ar + e^- \rightarrow Ar^+ + e^- + e^- \qquad (2.33)$$

Because of the mechanism of the collisions between ions and target atoms had been discussed in the previous section of this chapter, there is no need to give more information about this phenomenon nonetheless it is believed that to note the dependency of the deposition rate of the thin film to the sputtering pressure and current. At the very low chamber pressure the sheath of the cathode becomes wider, which results in the producing ions far from the cathode (target). The mean free path of electrons are large and electrons which are accumulated by anode are not replenished by ion – strike – induced secondary electron emission at the cathode. Herewith the efficiency of ionization is low and self-maintained discharge may not be conserved around 10 m torr pressure. By increasing the pressure at fixed voltage the mean free path, which electron has, shows decrease, more ions can be generated and the current flow becomes larger. But if the pressures riches very high levels the efficiency of deposition becomes worse (Ohring 2001). See the figure below.

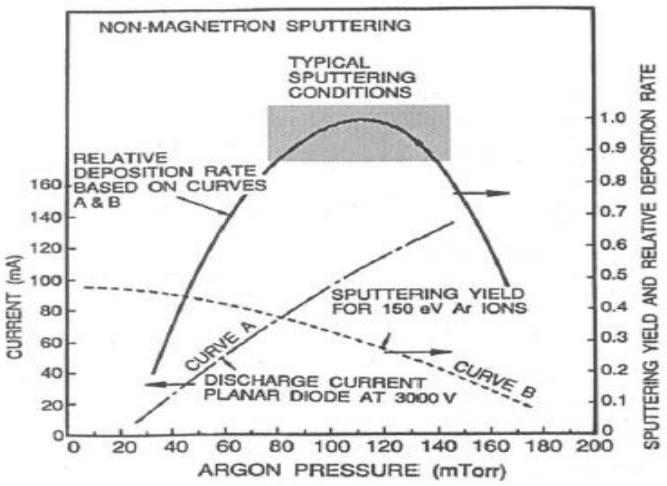

Figure 2.24. Working pressure, current and deposition rates relation in non-magnetron DC sputtering (Source: Kern 2012).

Film growth rate may be determined as following formula.

$$G\left(\frac{cm}{s}\right) \approx \frac{\mathbb{W}\,ג}{g\rho(1+\gamma)E} \tag{2.34}$$

Where G is the growth rate, $\mathbb{W}$ is discharge power density (W/cm^2) , ג is the mean distance from the cathode sputtered atoms travel before they become thermalized, g is the distance between cathode and anode, ρ is the atomic density, γ is the secondary electron emission co-efficient and E is the average sputtering energy.

2.3.3.2.2. Radio Frequency (RF) Sputtering

Radio frequency; known as an alternating current within a particular frequency range. Although there is no certain border between radio waves and microwaves, typically RF frequency in a range of 50 kHz to 100 MHz. 13.56 MHz is the most common radio frequency.

If dielectric materials such as SiO_2, ZrO_2 are used as target in DC sputtering technique the required potential to deposition can be reach extremely high values (~10^{12} V) (Ohring 2001). Hence it is not preferred to use DC technique when depositing insulator / semi – conductors. To perform the sputtering of dielectric materials RF sputtering technique has been developed (Maissel). See the figure below.

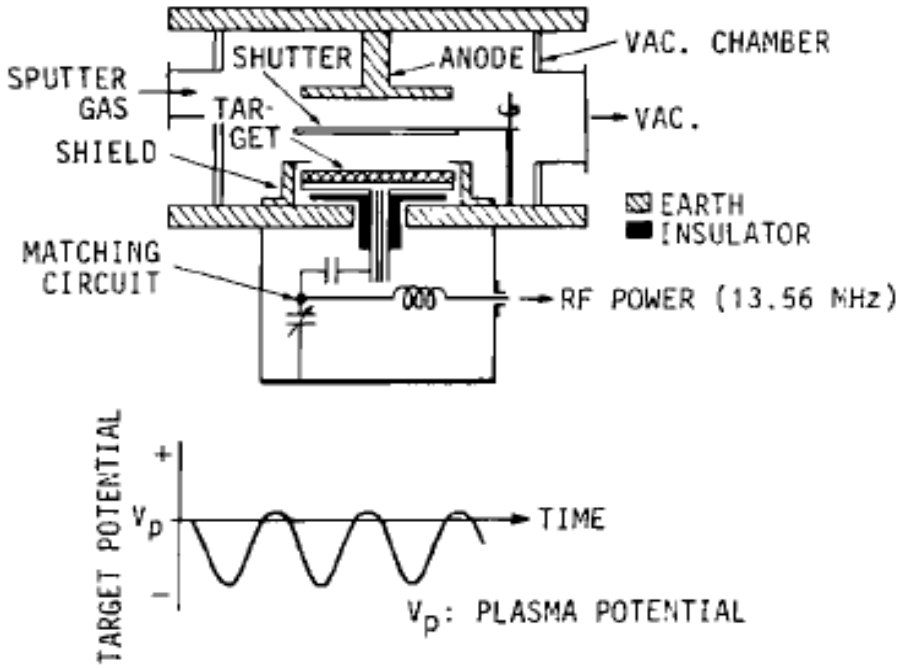

Figure 2.25. RF sputtering.
(Source: Wasa and Hayakewa 1992)

In RF sputtering technique it is possible to maintain a gas discharge at very low pressure such as 0.5 -2 Pa by means of high frequency. To increase the impedance of the glow discharge, which is created by RF source, an impedance matching network is required. An impedance matching network may increase the impedance from 50 Ω to in the order of some kΩ. Note below figure. Due to working mechanism of this network is beyond of the scope of this thesis, it is not going to be discussed.

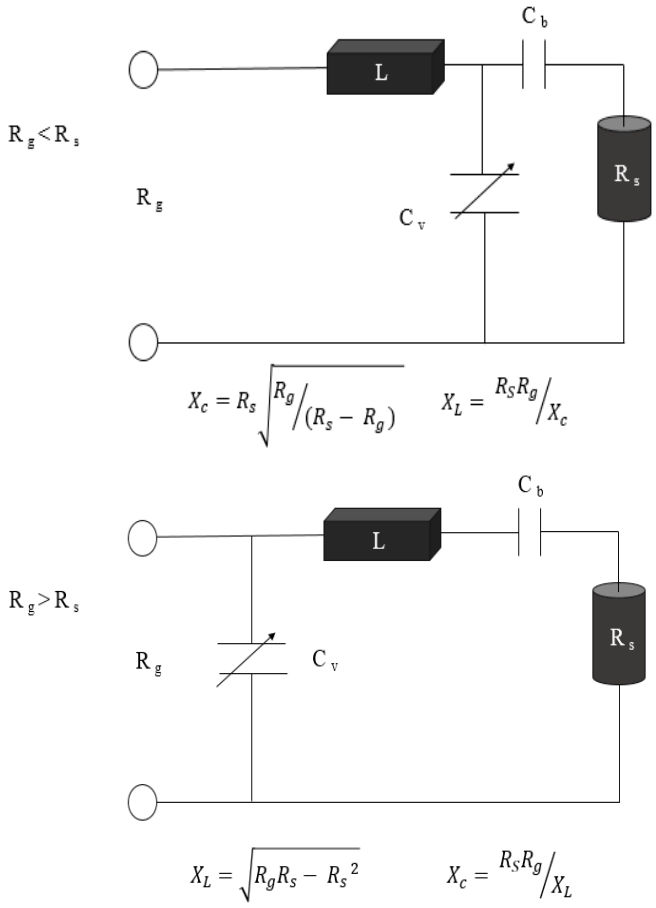

Figure 2. 26. The impedance matching network of RF sputtering
(Source: Wasa and Hayakewa 1992).

In RF sputtering system, working pressure may be as low as 1 mtorr because the electric field, which is created by RF, causes an increase of the collisions between ionization gas molecules and secondary electrons. In this technique increasing of the frequency causes an increase of the current on target (Wasa and Hayakewa 1992). Target current density may be given as following formula. R g

$$I_S \approx C\frac{dV}{dt} \tag{2.35}$$

I_S : Current density.

C : Capacitance between plasma and target.

$\frac{dV}{dt}$: Time variation of target potential.

2.3.3.2.3. DC and RF Magnetron Sputtering

The logic behind of the magnetron sputtering is creating a trap to the electron or ion to increase the collision between secondary electrons and ions which aims to get higher sputter yield. To incorporate magnets into the game, they are buried just under the target material. In the figure 2.27 different magnetron sputtering target, which have different geometry, is represented.

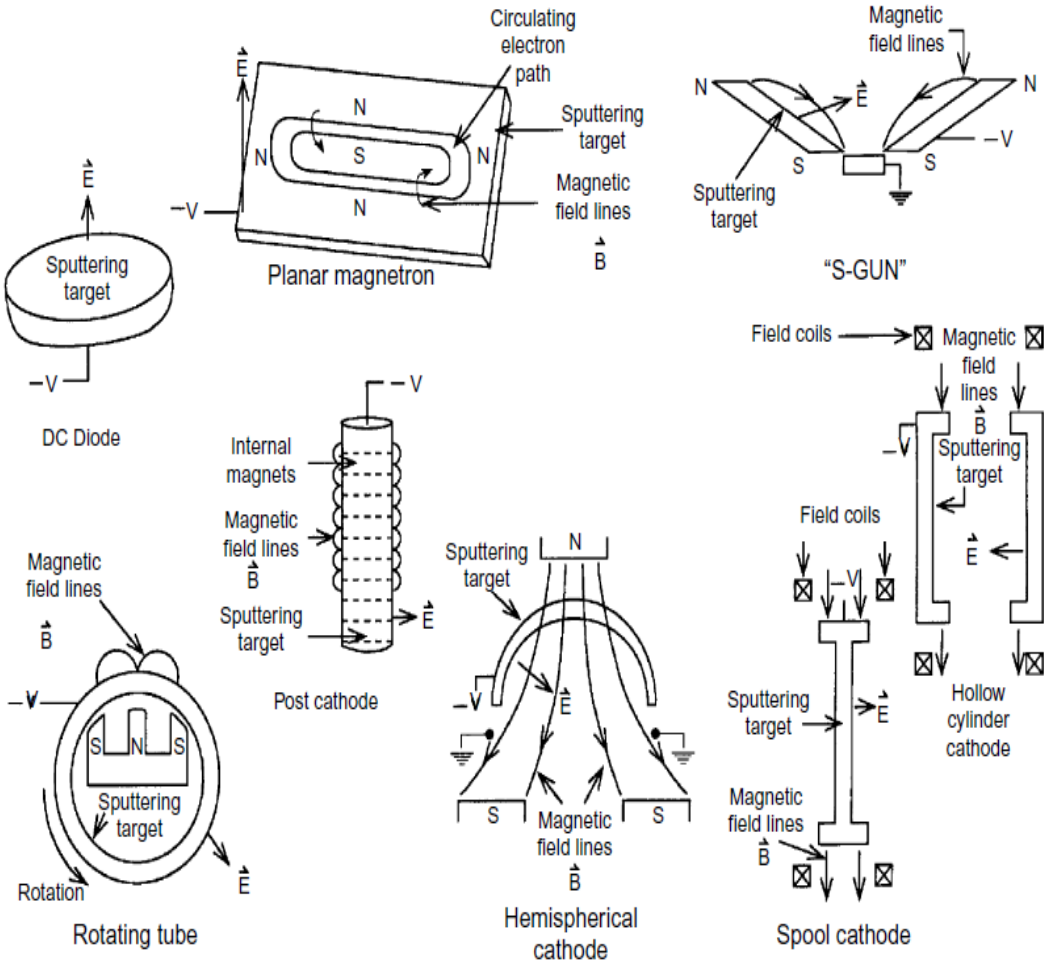

Figure 2.27. Sputtering target configurations.
(Source: Mattox 2010)

To understand the impact of the magnetic field on ions let us focus on planar magnetron sputtering. See the figure below.

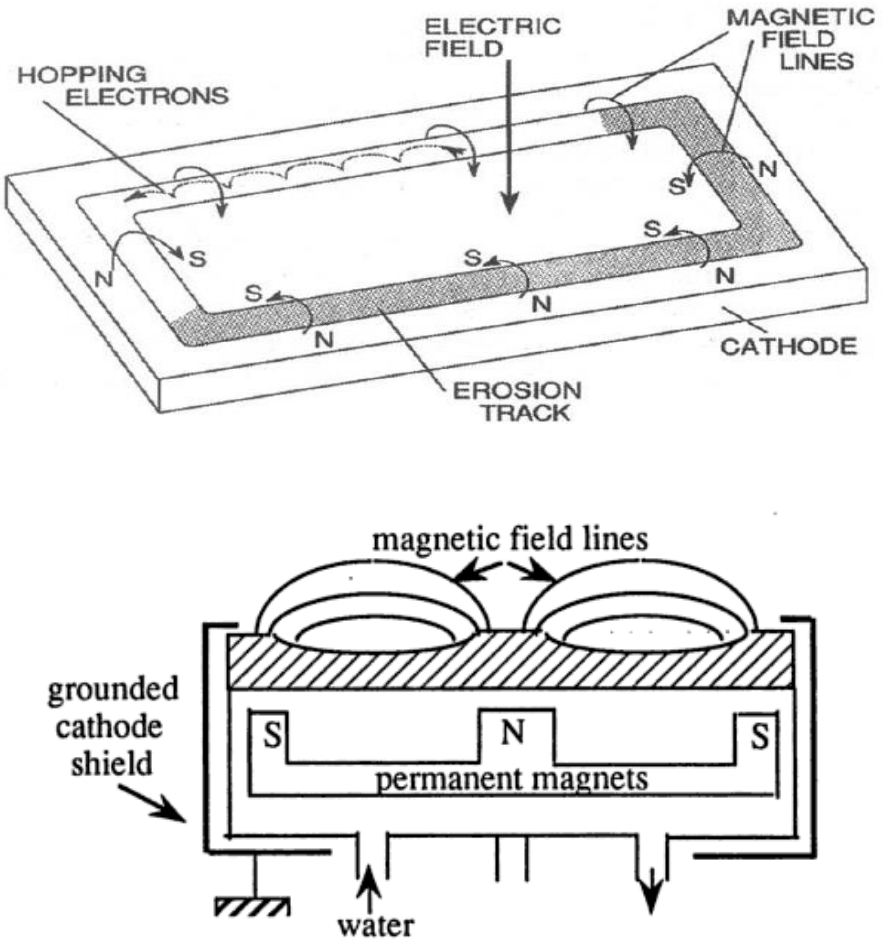

Figure 2.28. Planar configuration of magnetron sputtering target.
(Source : http://web.iitd.ac.in/~sujeetc/PHL702_2015_L16.pdf 2015)

As it may be clearly understood from the figures above, the magnetic field creates a parabolic path (hemi circle) between the poles of the magnets on which the electrons travel. Those hemi circles have a radius r. This hoping radius might be determined by following formula.

$$r \sim \frac{1}{B}\sqrt{\frac{2m}{e}}\,V_d \tag{2.36}$$

Where V_d is voltage drop across dark space (~ 100 V), B is the magnetic field with the magnitude 100 G

Typically radius for e^- ~ 0.3 cm for Ar^+ 81 cm.

According to the magnetic fields created, the magnetron sputtering systems can be determined in three types. See the figure below

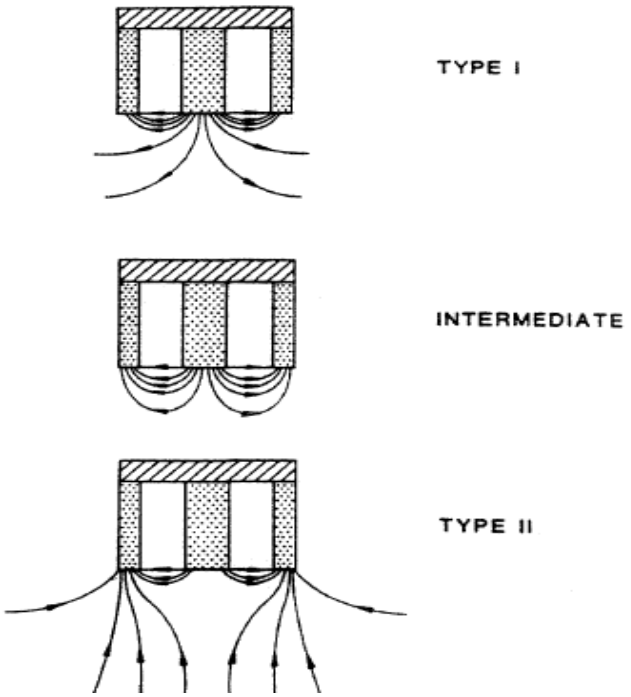

Figure 2.29. Magnetron configurations Type-I (unbalanced). (Middle) Intermediate (balanced). (Bottom) Type-II (unbalance)
(Source: Kadlec and Musil 1996).

As a result;

Deposition pressure: 10^{-5} to 10^{-3} torr

Deposition rate : 0.2 ~ 2^{-6} m/min,wich is correspons to 10 times higher than conventional sputtering.

Deposition temperature: 100 – 150 ^{o}C

Further information about magnetron sputtering is beyond of this thesis therefore it is not going to be analyzed in detail.

2.3.3.3. Reactive Sputtering

Reactive sputtering is nothing but deposition metallic target in the presence of any reactive gas besides Ar. Various dielectric materials can be deposited using different reactive gases. (Or mixtures) See the below table.

Table 2.7. Conventional compounds reactively sputtered.
(Source: Ohring 2001)

Oxides (R_g: Oxygen)	Al_2O_3	In_2O_3	SnO_2
Nitrides (R_g: Nitrogen, ammonia)	TaN	TiN	AlN
Carbides (R_g: Methane, acetylene)	TiC	WC	SiC
Sulfides (R_g: H_2S)	CdS	CuS	ZnS

Where R_g is reactive gas

In this technique reaction is occurs only at the target surface and on the substrate, it also occurs on the walls of the chamber which behaves as anode. See the figure below.

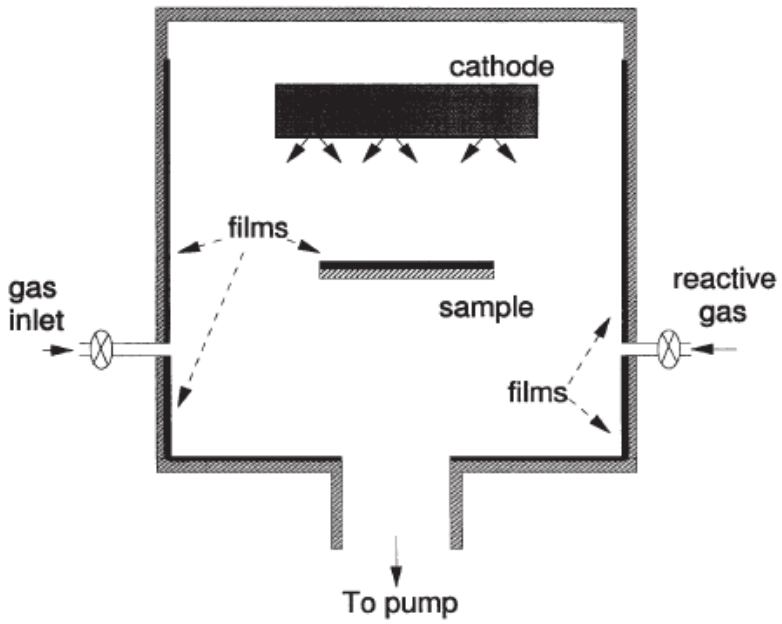

Figure 2.30. Reactive deposition system (Most basic form).
(Source: Seshan 2012)

Besides that, the chemical reaction, which forms metal oxides from metal target atoms by reactive gas atoms, does occur rarely in the flight of atoms, it occurs between purely, simply and freshly deposited target atoms and reactive gas atoms on the thin film surface. On the other hand forming a composition on the cathode may remarkably alters the process of sputtering, which can be accepted as a disadvantage of this technique.
Using the alteration in the kinetics of discharge, the working principle of this technique may be explained. See the figure below.

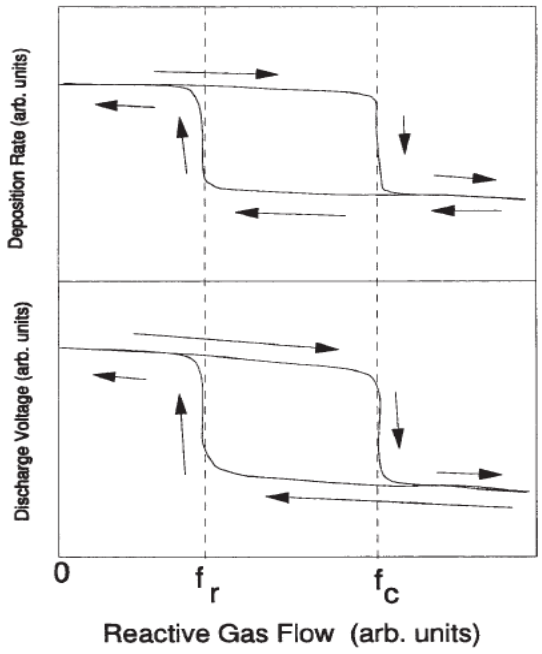

Figure 2.31. The deposition rate and the discharge voltage relation as a function of reactive gas (constant pressure) (Source: Seshan 2012).

If there is no reactive gas flow, the target material is being impinged only by Ar atoms (indicates left side of the above chart) and as a result of this the deposition forms as metallic. By increasing the reactive gas flow, the oxidation of the film is starts at a certain point (critical flow point) and stoichiometric oxides are formed. After that point the film is not capable of absorb more reactive atom, and the atoms (O_2) form as an oxide layer on the thin film on the cathode, causing a decrease in the sputter yield (Seshan 2012). To create reaction on the cathode and anode, an optimum concentration of reactive gas is needed. See the following equations.

$$k \frac{N_g}{N_c} > 1 \quad \text{Reaction at cathode} \tag{2.37}$$

$$k \frac{N_g}{N_s} > 1 \quad \text{Reaction at substrate} \tag{2.38}$$

Where N_g is the reactive gas molecules that impinge a unit area of target surface per unit time, N_c is the number of the sputtered atoms from target per unit time, N_s is the number of deposited atoms / molecules per unit area per unit time.

CHAPTER 3

EXPERIMENTAL

3.1. Motivation

Starting with the invention of CdO (Transparent conductive oxide) thin film, which was prepared by thermal oxidizing vacuum sputtered from cadmium metal in 1907 by Baedeker, transparent conductive oxides have become more and more interested material used in advanced technological applications such as, transistors, solar cell, light – emitting diodes (LCDs), antistatic coatings, electromagnetic shielding. By enourmous augmentation of interaction between humankind and technological devices, display devices have become essential for visual communication. The information which is to be delivered via a technological device would be usually in the form of color images. Electrochromic displays device (ECDs) is one of the most powerful candidate for this purpose and they have numerus features such as multicolor, high contrast, optical memory, and no visual dependence on viewing angle (Monk, Mortimer, and Rosseinsky 2008). Besides ECDs, electrochromism phnomenon is also in used in smart glass technology and intelligent textile applications. Among all ECDs applications intelligent textile comes to the forefront in military industry (Camuflage,dedector) or even in communucation, and in fashion industry where it is used as color changing materials. A deep litrature survey has proven that glass or flat polymer surfaces are used as substrate, which limits the application fields or variety. Due to this limitation a huge demaned has appeared in EC textile technonolg. In the scope of this thesis it is aimed to deposit ITO on cylindrical polyamide surface to construct electrochromic fiber.

3.2. Structure of Electrochromic Fiber

In the most general sense an electrochromic material consist of seven layers (See figure 2.4) by showing variations depending on the desired application: Substrate / TCO / Ion storage thin film / Ionic conductive layer / Electrochromic thin film (EC layer) / TCO / Substrate. Optical modulation of electrochromic layers (Ion storage layer and electrochromic layer) results from the oxidation and reduction reaction between them. According to the scope of this thesis, a cylindrical surface (as substrate) is used. Figure 3.1 represents the structure of electrochromic fiber.

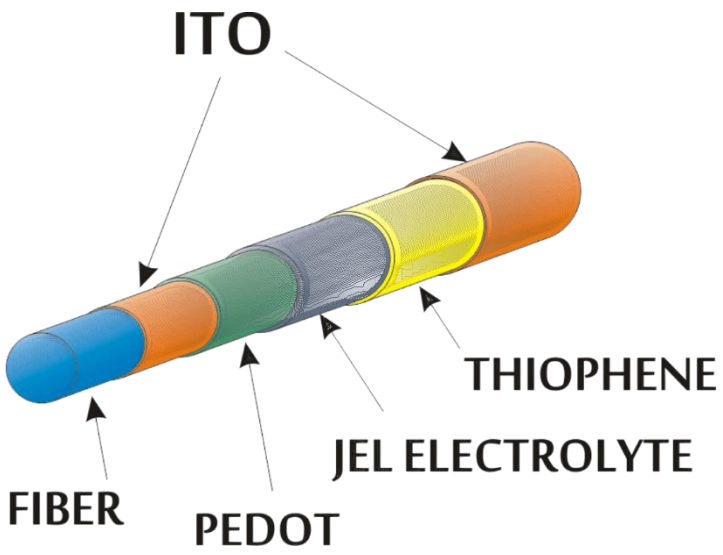

Figure 3.1. Structure of electrochromic fiber.

In this structure, polyamide fiber with diameter 150 µm is substrate, ITO thin film is contact layer, PEDOT is electrochromic thin film (EC layer), Jel electrolyte is ionic conductive layer and thiophene is used as ion storage layer. The reduction and oxidation reactions occur between thiophene and PEDOT which result in the modulation of optical properties of the structure by means of jel electrolyte.

3.3. Material Type

3.3.1. Inverted Cylindrical Magnetron Sputtering (ICM)

Roll to roll inverted cylindrical magnetron sputtering is nothing but a redesigned form of the conventional magnetron sputtering (Notice chapter 2). According to the scope of the thesis a, roll to roll inverted cylindrical magnetron sputtering (DC) system (ICM is the best candidate for deposition three-dimensional shapes (Ohring 2001).) is designed for deposition indium doped tin oxide on cylindrical polymer surface homogeneously. See figure 3.2.

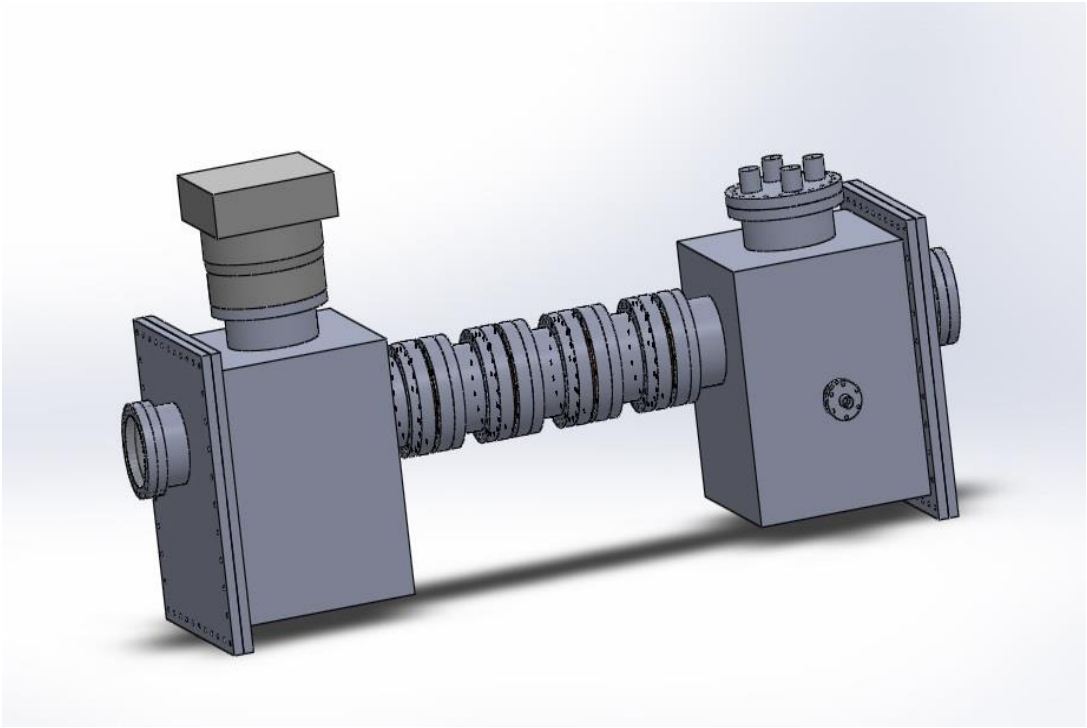

Figure 3.2. Roll to Roll Inverted Cylindrical Magnetron Sputtering system design.

Unlike the conventional magnetron sputtering system, a planar substrate is used as target material. In cylindrical magnetron sputtering system, a ring shaped target is used. And due to dependency on the geometry of the target material, different sputtering directions may be obtained by different shaped targets (See figure 2.7). Resulting in the shape of the target material, a cylindrical shaped plasma is obtained, so ejected target atom will go towards the center of cylinder where the polyamide fiber is located.

3.3.2. In_2O_3: Sn (ITO)

Indium tin oxide (tin doped indium oxide) is the most commonly used n-type TCO due to its magneficiant combination between transmittance at the visible region of spectrum and the high electrical conductivity. Beside that it has environmental stability. In the table 3.1 the basic properties of ITO are listed.

Table 3.1. The characteristic features of tin doped indium oxide.
(Source: Dawar et al. 1995)

Electrical conductivity σ (Ω^{-1} cm^{-1})	30 – 2.3 x 10^4
Carrier concentration n (cm^{-3})	10^{20} - 10^{21}
Hall mobility μ_H (cm^2 V^{-1} s^{-1})	10 - 70
Tranmission at visible spectrum range (%)	85 - 95
Reflection at infrared region (%)	80 - 90
Energy band-gap (eV)	3.0 – 4.6
Refractive index	1.8 – 2.1
Effective mass	0.30 – 0.35
Theoretical density (g/cm^3)	7.12

Tin doped indium oxide is a composition of In_2O_3 and SnO_2, 90:10 wt. % respectively and it is transparent and colorless in thin film, whereas in bulk form it is yellowish to grey. The magnificent features of ITO are based on it is chemical structure which is cubic bixbyite (Similar to In_2O_3 crystal structure) See figure 3.3. Doping of In_2O_3 with Sn; doped Sn atoms replaces In^{3+} in the structure of indium oxide which results in forming an interstitial bond between Sn and oxygen, and also formed both as SnO_2 and SnO; accordingly it has a valency of 4+ or 2+ respectively. A reduction appears in carrier concentration resulting from the lower valence state, since a hole is created which acts as a trap and reduces conductivity. Besides that, the prevalence of the SnO_2 state means Sn^{4+}, which acts as an n-type donor releasing electrons on to the conduction band. However, in ITO either substitutional tin atoms or oxygen vacancies have significant contribution on the conductivity, and the material can be represented as $In_{2-x}Sn_xO_{3-2x}$.

In that structure one unit cell contains 16 units of In_2O_3 herewith, for defect free indium oxide crystal, there are 80 atoms in one unit cell of ITO (Bashar 1998). The lattice parameters at the range of 10.12 – 10.31 Å, which shows variation with Sn doping (Nath et al. 1980).

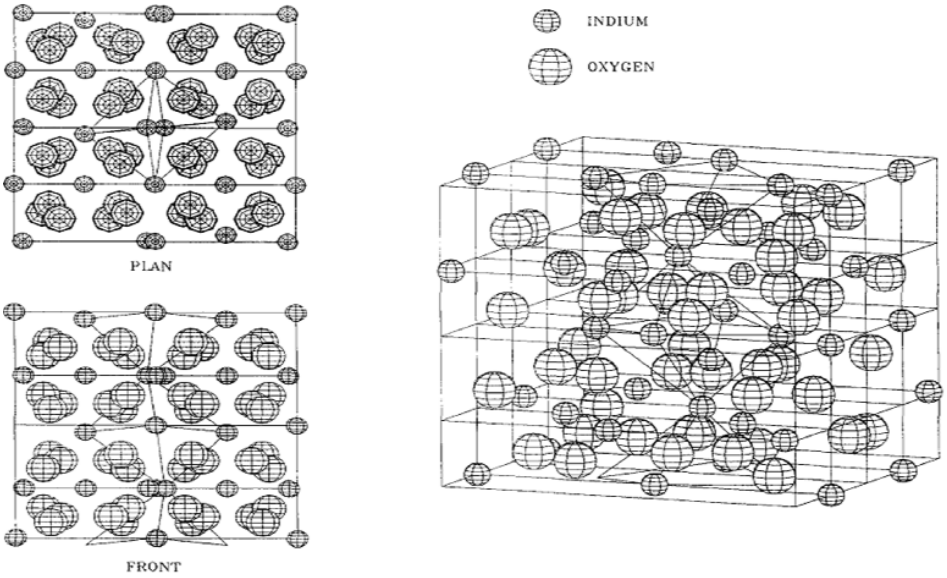

Figure 3.3. In_2O_3 crystal structure.
(Source: Kim et al. 2013)

Indium oxide structure comprises of either d-site crystallization or b-site crystallization simultaneously. Notice figure 3.4.

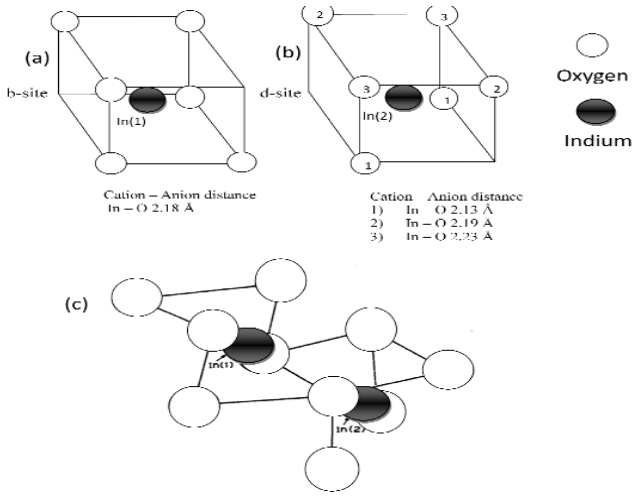

Figure 3.4. b-sites (a), d-site (b) and combination of these two sites (c) of ITO.
(Source: Marezio 1966)

To deposition ITO on cylindrical surfaces a specially designed cylindrical target is needed (Notice chapter 2.4. and 3.3.1.). In the figure 3.5 cylindrical ITO target is shown.

Figure 3.5. Special designed cylindrical ITO target.

3.3.3. Polyamide (PA)

Polyamide in other word nylon is a semi-crystalline polymer. PA is consists of monomers which are linked via peptide bonds. Nylon 6 and nylon 66 are the most conventional types, in which the numbers refer to the number of methyl groups. See the figure below.

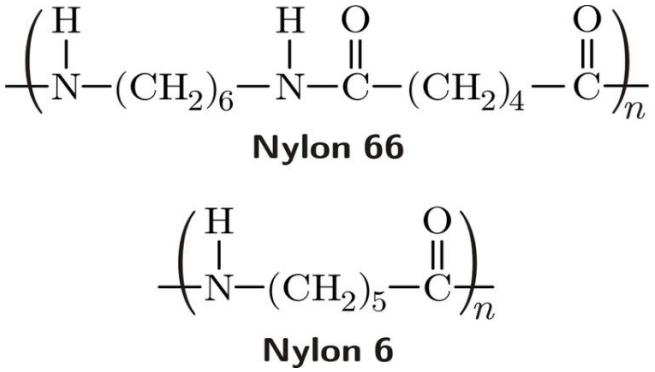

Figure 3.6. Chemical structure of polyamide 66 and polyamide 6.

Polyamides have an extremely large application fields in engineering due to the features they have such as low permittivity to the gases, excellent wear resistance, high mechanical resistance and high resistance to some chemicals. They are mostly formed into fibers and are used for monofilaments and yarns. In the scope of this thesis monofilament nylon 66 is used as a substrate because of its good adhesion and bonding properties. In table 3.2 the basic properties of polyamide is listed.

Table 3.2. Basic properties of polyamide

Density g/cm^3	Thermal Coefficient of expansion	Tensile Strength N/ mm^2	Max Cont. Use Temp. ^{o}C
1.13 – 1.31	90 – 20 / 70 x 10^{-6}	90 – 185	150 – 185

3.4. Experimental Setup

3.4.1. Inverted Cylindrical Magnetron Sputtering System Setup

The roll to roll inverted cylindrical magnetron sputtering (Figure 3.2) is represented in the figure 3.7 with its side equipments to run the deposition of ITO on fiber with accuracy to get desired results.

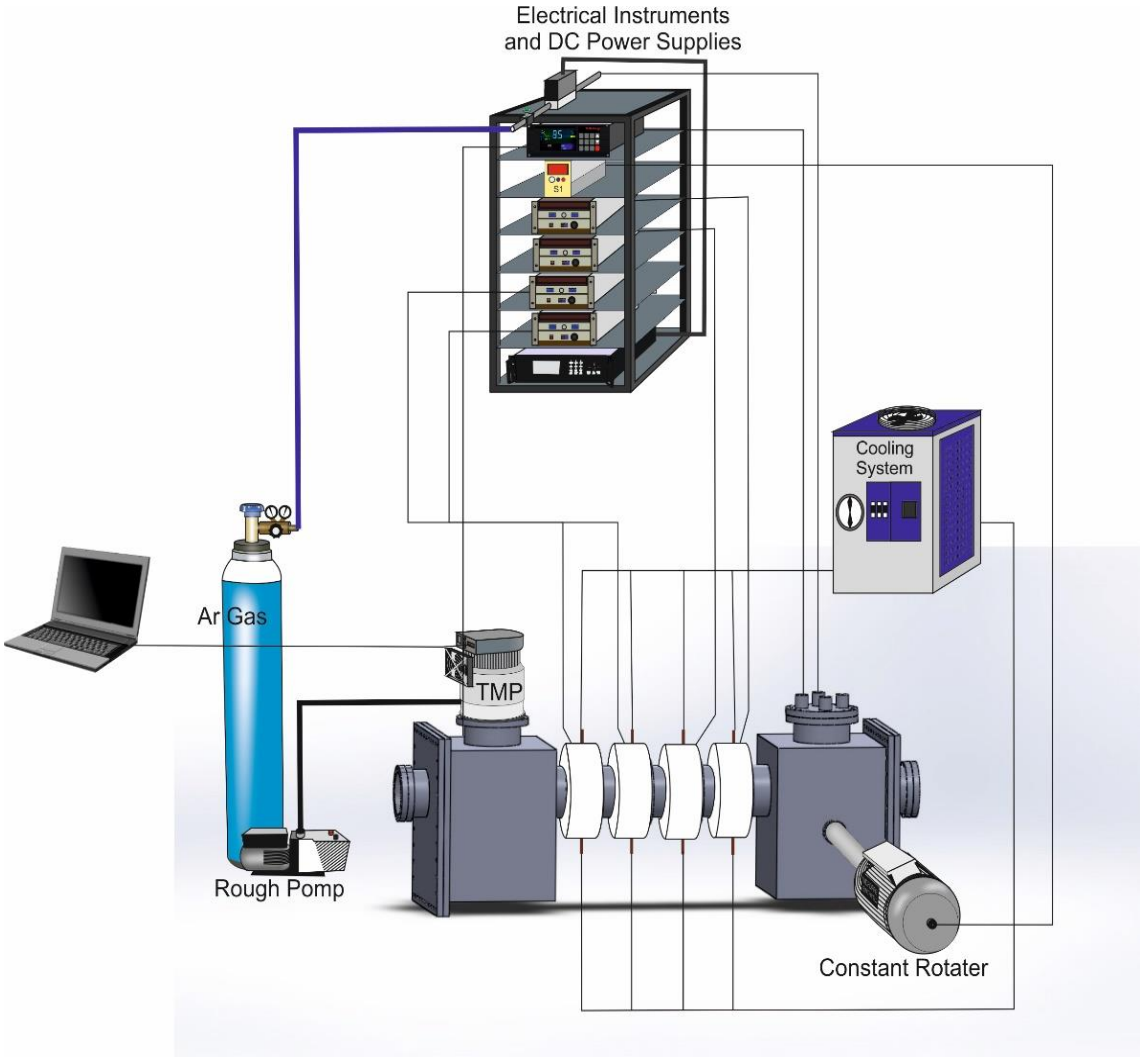

Figure 3.7. Roll to Roll Inverted Cylindrical Magnetron Sputtering system setup.
(Source: Taşdemir 2015)

Because of the nature of the physical vapor deposition technique, it is needed to get high vacuum levels, as it might be clearly noticed from figure 3.6. either rough pump (Which decreases pressure level on the order of 10^{-3} torr) or turbo molecular pump (That decreases the pressure level on the order of 10^{-6} torr, which is proper vacuum level for quality thin film deposition) are used, it can also be recognized that Ar gas is used as ionization gas and the gas flow is controlled by flow meter, which can be seen in the figure 3.7 either, in addition these, side equipments should be used as cooling mechanism in order to keep the temperature of the ITO target at around room temperature, which may be seen in the same figure. Finally a constant rotator is used to transfer fiber from left chamber, where uncoated fiber is stored in right chamber, where ITO coated fiber is restored.

3.4.2. Electrochromic Fiber Production Setup

According to the scope of thesis, only basic information is given about whole electrochromic fiber process. The reader can see elctrochromic fiber productions setup in the figure 3.8.

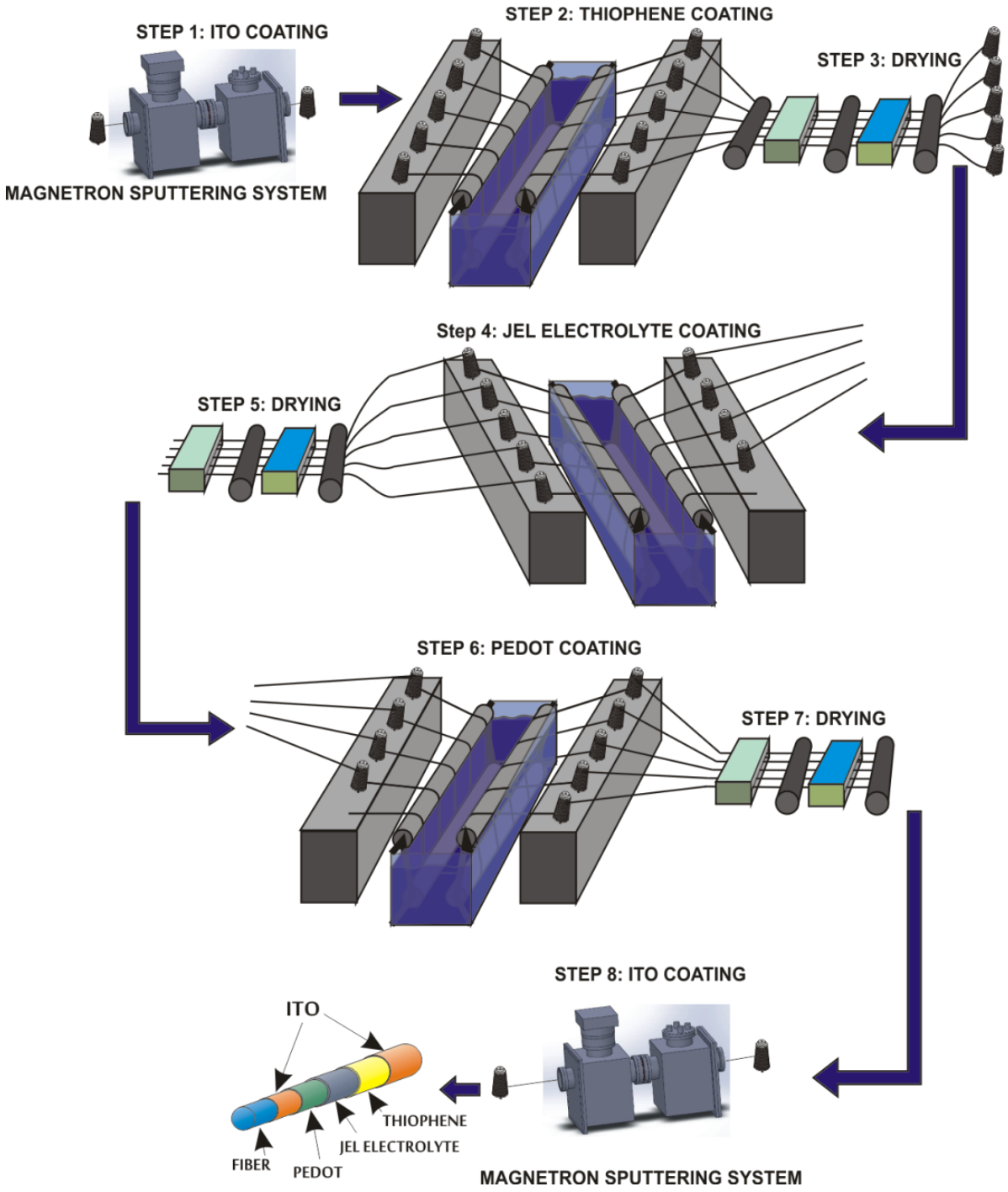

Figure 3.8. Electrochromic fiber production set-up

3.5. Experimental Process

Roll to roll inverted cylindrical magnetron sputtering system has mainly three parts, which is seen in the figure 3.9. The first one is fiber loading chamber (Which is shown on the left hand side), second is ITO deposition cylindrical target area (which is located between two chambers) and last one is fiber unloading chamber, that is seen on the left hand side .

Figure 3.9. Roll to roll inverted cylindrical magnetron sputtering system which is used in the scope of the thesis.

Deposition process: The process start with the evacuation of system in the range of 10^{-6} torr using rough pump and turbo molecular pump, respectively. After reduction the pressure to the apporiate level,the ioniztion gas is injected to the system usind a gas flow meter . And a DC voltage is applied to create Ar^{+} plasma (Plasma generated during magnetron sputtering is represented in the figure 3.10) Following that, polyamide fiber is passed through the plasma by the means of apparatus that have 16 rollers, which means the fiber cycles 15 times in the plasma region. The process is ended by unloding the ITO coated fiber in the right hand side chamber.

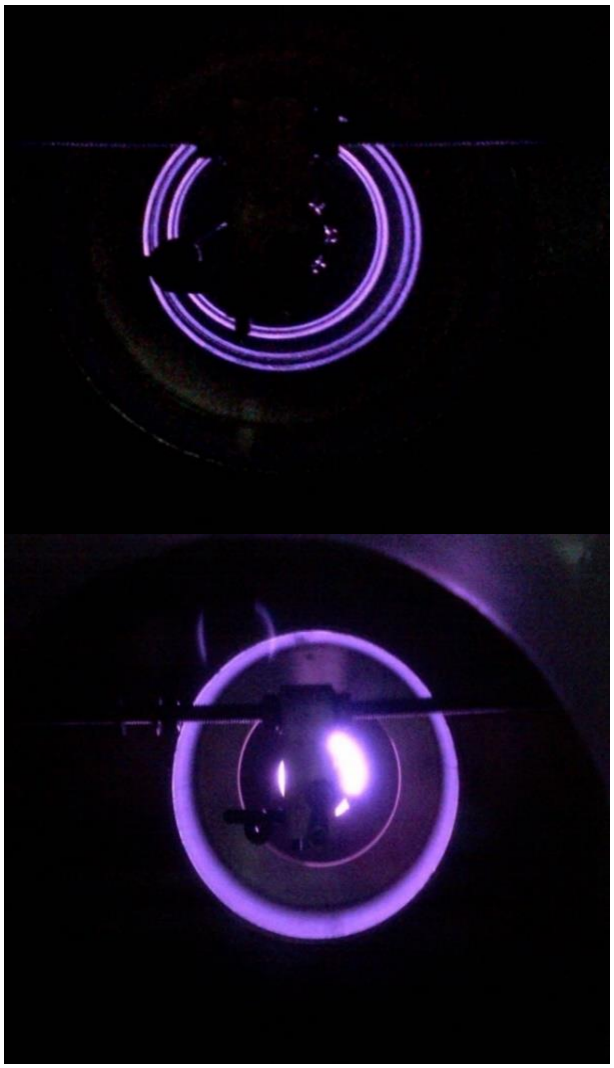

Figure 3.10. During deposition; polyamide fibers passing through the target plasma zone.

In conventional magnetron sputtering system the thickness (Consequently the quality of the thin film) depends on the deposition time as well as the temperature of suctrate, vacuum chamber pressure etc. But in roll to roll magnetron sputering, the thickness of the film is not directly depend on time since the sample is passed through the plasma region by means of different apparatures, in other words the sample is in a motion. According to the scope of this thesis different depositions (By varying ionization gas pressurea and DC power,) were handled to optimize the system to get apporiorate quality ITO coated fiber for ECD. The results are listed in the following chapter.

3.6. Characterization Procedures

3.6.1. Structural Characterization

3.6.1.1. Optical Microscopy Analyzes

Light microscopy systems can be basically categorized into six as bright field optical microscopy, oblige illimunation, dark fiel optical microscopy, phase contrast optical microscopy, differential inerference contrast microscopy and confocal laser scanning microscopy according to their area of utilazation. In order to observe the roughness and homogeneity of surface of ITO thin film, which is deposited onto polyamide fiber, a Nikon ECLIPCE LV 150 optical microscope is employed at clean room in physics department at IZTECH.

3.6.1.2. Scanning Electron Microscopy (SEM) Analyzes

Scanning electron microscopy has an important place in today's technology especially in semiconductor industry due to its remarkable features such as resolution quality, higher magnification and larger depth of field. Unlike traditional light microscopy, high energy electrons are used to dedect (produce image) the surface of the material. In the most general sense a beam of electrons (which are gained high energy) are focused on the sample in order to generate a variety of signals. The image is constructed by analyizng those signals (See chapter 2 for detailed information). According to the scope oh the thesis scanning electron microscopy (Quanta 250FEG scaning electron microscopy) is used at IZTECH Materials Research Center to investigate etiher non-coated polyamide fiber and ITO coated polyamide fiber surfaces.

3.6.2. Thickness Measurements

3.6.2.1. Thickness Measurements via Deposited ITO Mass

In order to calculate ITO thin film thickness by deposited tin doped indium oxide mass the density of ITO is needed (Notice table 3.1). This calculation is done using following formula.

$$\rho = \frac{m}{v} = \frac{\Delta m}{2\pi r l t} \tag{3.1}$$

Where ρ is the density of ITO, m is the mass of the coted or uncoated fiber, Δm is the mass difference between coated and uncoated fiber, l is the length of the fiber, t is the thickness of the thin film. In order to run that formula, the weight of 10 meters polyamide fiber is measured before and after deposition, the difference between them leads us to define the thickness of the thin film.

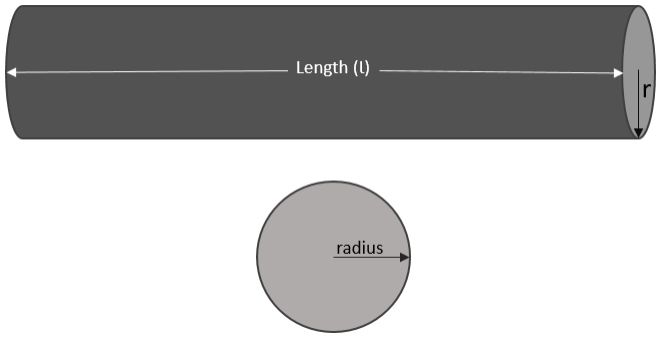

Figure 3.11. Representation of ITO deposited polyamide fiber

3.6.2.2. Thickness Measurements via Calibration Sample.

Another thickness measurement method is, simulating the polyamide fiber with the (Almost) lamellae shaped in the same way. In this technique a piece of lamellae, which is shaped as fiber (0.5 cm width, 5 cm length), is located ICM plasma area and deposited with the same parameters. After deposition, it is possible to measure the thickness using profilometry.

3.6.2.3. Thickness Measurements via SEM images

An alternative thickness measurement method is measuring the diameter of un-coated and ITO coated fiber. Notice the following equation.

$$t = \frac{\Delta d}{2} \tag{3.2}$$

Where Δd is the diameter difference between un-coated and coated fiber, t is the thickness of the film.

3.6.3. Electrical Characterization

The resistance of ITO coated fiber is measured using digital or analog multimeter (ohmmeter). The measurement is performed using following equation.

$$R = \frac{V}{I} \tag{3.3}$$

Where R is resistance of the material, V is the applied voltage, I is the current which passes through the material. There are two parameters which have a direct effect on the resistivity of the material as material type (what made of) and the geometry of the material. Notice figure 3.11.

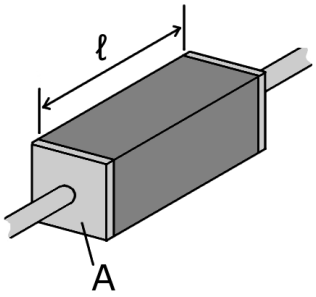

Figure 3.12. Representation of cross-section area and length of bulk resistivity

It is clear that there is a relation between resistance and resistivity with following bulk formula.

$$R = \rho \frac{l}{A} \tag{3.4}$$

Where R is the resistance of the material, ρ is the resistivity of the material, A is the cross-section area of the material (cm^2).

CHAPTER 4

RESULTS AND DISCUSSIONS

According to the scope of the thesis, tin doped indium oxide (ITO) has been deposited onto the monofilament polyamide fiber which has 150 μm diameter, as the contact layer of electrochromic fiber. Although there are enormous number of articles on the deposition of ITO (or TCOs) thin films on flat (Large scale) polymer substrate, there is no published article on deposition of TCOs thin films onto the cylindrical polymer surfaces. Before starting the deposition onto the polymer surfaces depositions onto the glass surfaces have been carried out in order to make sure if the target material and the roll to roll inverted cylindrical magnetron sputtering system are proper to deposition onto the polymer surface. See the table below.

Table 4.1. Deposition parameters on to the glass substrate.

Sample Name	G2	G3	G4
Gas flow (sccm)	150	150	200
Deposition Pressure (10^{-3} torr)	6.87	6.90	5.70
Power (Watt)	40	40	30
Deposition time (min.)	10	10	10
Surface Resistance	1.5 MΩ	13 kΩ	0.5 MΩ

In figure 4.1 the reader is able to see the pictures of the deposition of ITO on glass.

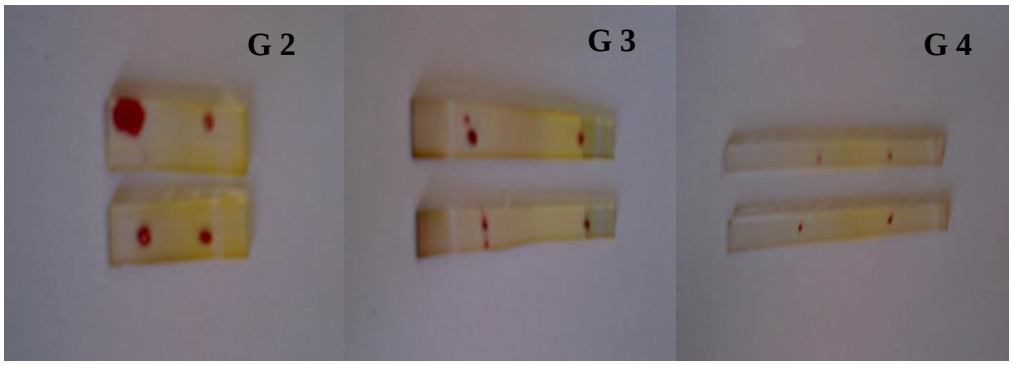

Figure 4.1. Optical microscopy image of ITO coated glass.

As it might clearly understood from the picture above the thickness of the ITO films on to the glass are not homogeneous, which in a range from 145 to 260 nm.

4.1. Inverted Cylindrical Magnetron Sputtering Optimization.

Literature survey has revealed that, there is no published article on ITO deposition onto cylindrical polymer surfaces (polymer fiber). For that reason, before starting the experiments, the ICM system should be optimized for deposition of ITO thin film. For that reason there some pilot scale test works have been carried out. The main purpose of pilot scale test works is to figure out, if deposition of ITO thin film onto polyamide fiber is possible or not. See the table below.

Table 4.2. Pilot scale test works deposition parameters

Sample Name	P 1	P 2	P 3
Gas flow (sccm)	150	100	125
Deposition Pressure (10^{-3} torr)	7.23	6.4	6.9
Power (Watt)	200	200	200
Rotator Velocity (cm/min)	119	119	119

In figure 4.2 the reader is able to see the pictures of pilot scale test works of deposition on ITO on PA fiber.

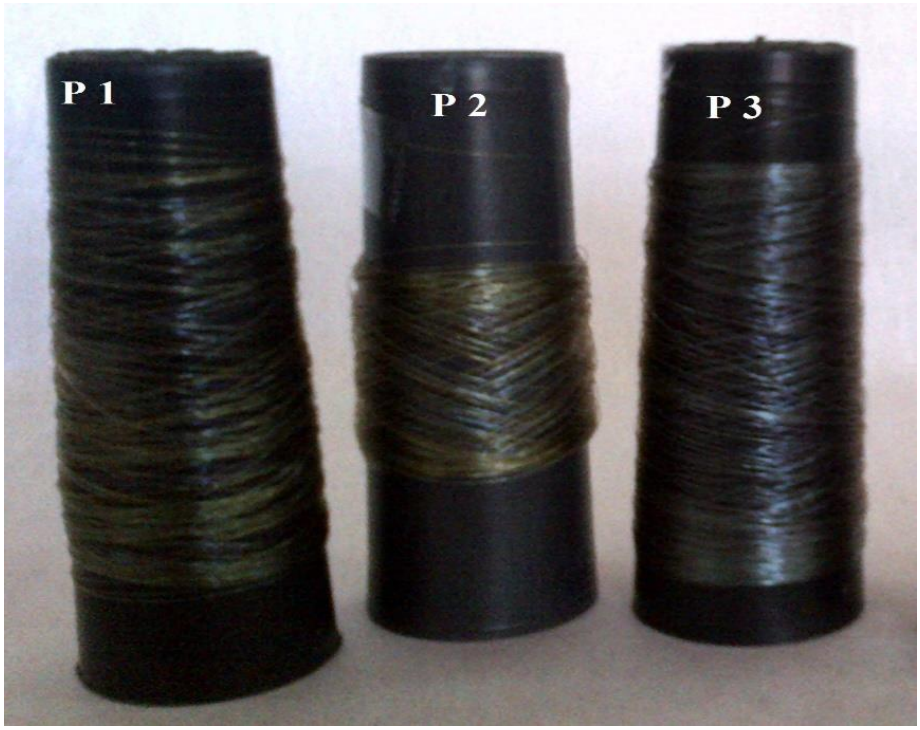

Figure 4.2. Pilot scale test works on ITO deposition on PA fibers

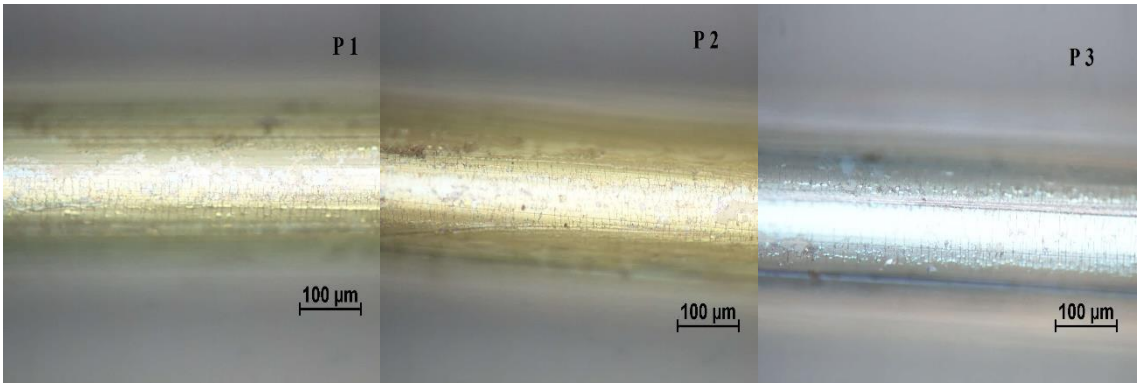

Figure 4.3. Optical microscopy image of pilot scale test works.

The electrical measurements of pilot scale test works were repeated 10 times for each sample and final electrical resistance is determined the mean (MR) of these values. The electrical measurements are given in the table 4.3 with their standard deviations and relative standard deviations. The standard deviation of the measurements have been carried out by formula 4.1. The relative standard deviations have been carried out by formula 4.2.

$$\sigma = \sqrt{\frac{\sum(x-\bar{x})^2}{N}} \tag{4.1}$$

$$RSD\ (\%) = (\frac{\sigma}{MR})\ 100 \tag{4.2}$$

Where σ is the standard deviation, x is the each measurement value, $\bar{x}$ is the mean of the values, N is the number of the measurement, RSD is the relative standard deviation and MR is the mean resistance value.

Table 4.3. Electrical measurements of the pilot scale test works.

Sample Name	P1	P2	P3
Measurement 1 (MΩ / cm)	2.4	1.4	2.3
Measurement 2 (MΩ / cm)	1.9	1.6	2.6
Measurement 3 (MΩ / cm)	2.8	2.3	1.7
Measurement 4 (MΩ / cm)	3.2	1.1	2.1
Measurement 5 (MΩ / cm)	3.6	2.0	2.3
Measurement 6 (MΩ / cm)	2.2	2.7	2.9
Measurement 7 (MΩ / cm)	2.7	1.1	1.6
Measurement 8 (MΩ / cm)	2.7	1.5	2.0
Measurement 9 (MΩ / cm)	3.4	1.9	1.9
Measurement 10 (MΩ / cm)	4.1	1.4	2.6
Mean Resistance (MΩ / cm)	**2.9**	**1.7**	**2.2**
Standard Deviation (MΩ / cm)	**0.6**	**0.5**	**0.4**
Relative Standard Deviation (RSD %)	**20.7**	**29.4**	**18.2**

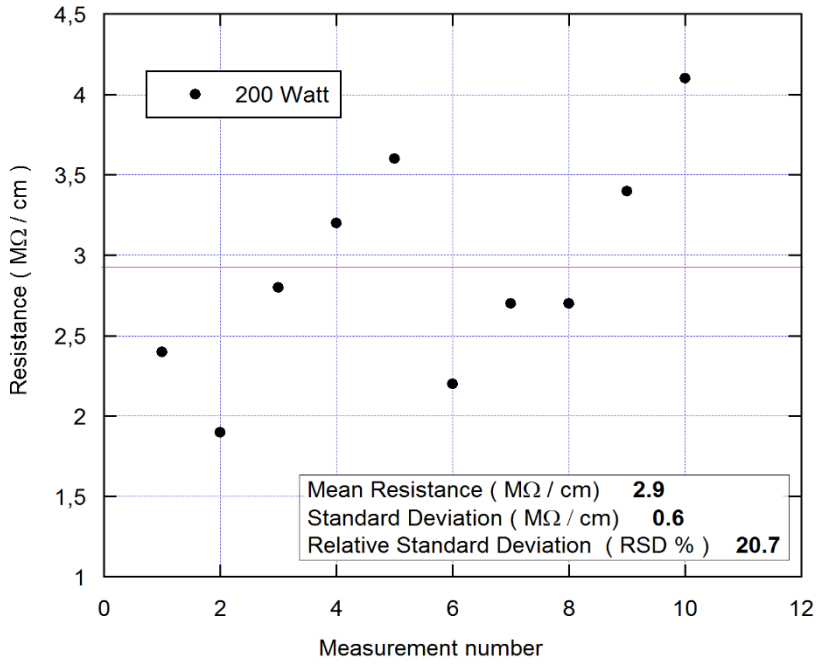

Figure 4.4. Resistance measurements of P1 pilot scale test work.

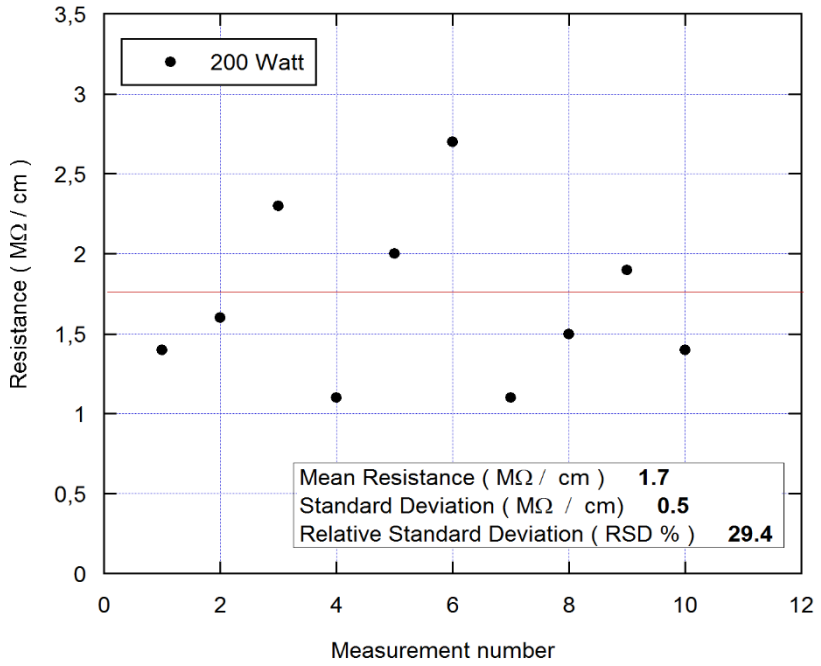

Figure 4.5. Resistance measurements of P2 pilot scale test work.

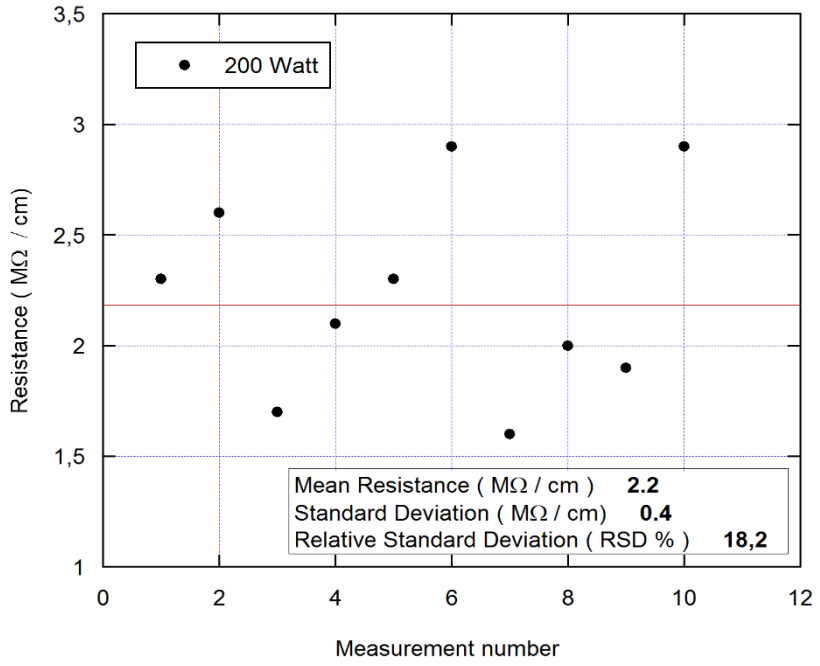

Figure 4.6. Resistance measurements of P3 pilot scale test work.

The electrical measurements and optical microscopy images indicate that, the deposition of ITO thin film on PA fiber might be done using specially designed ICM.

4.2. Studied Parameters

As it was mentioned in chapter 2 there are some variables, which have direct effect on the quality (Figure of merit) of the deposited thins film. Those variables are mainly, Substrate temperature of the sample, ionization gas pressure, the energy of the sputtered target atoms, substrate target distance and the ability of bonding of sputtered target atoms with the substrate surface. According to the scope of the thesis the studied parameters are; the pressure of the ionization gas and the applied power. Although substrate temperature has a very crucial role on the quality of the TCO thin films (Detailed information in chapter 2), the effects of it might not be worked, since it is not possible to control the substrate temperature of polyamide fiber due to its melting point, which is relatively low (~ 150^{o}C). As a first step while the pressure of ionization gas (Ar) was fixed at 100 sccm, the applied power had been changed at the range of 30 – 130 W with 10 W steps. After figuring out the proper power range for electrical resistance (It is discussed in the electrical characterization section) the power was fixed and the Ar gas pressure was changed at the range of 40 – 90 sccm with 10 sccm steps for the same purpose.

4.2.1 Structural Characterization Results

4.2.1.1. Optical Microscopy Results

ITO coated polyamide fiber acts either convex mirror or concave mirror simultaneously because of it is cylindrical shape. Therefore there occurs many diffraction and reflections on the structure (Detailed information (Rosendahl 1962), (Ohring 2001).), causing to appear in different colors. Figure 4.5 shows the optical microscopy images of ITO coated fibers with different deposition parameters (The deposition parameters are listed in table 4.3).

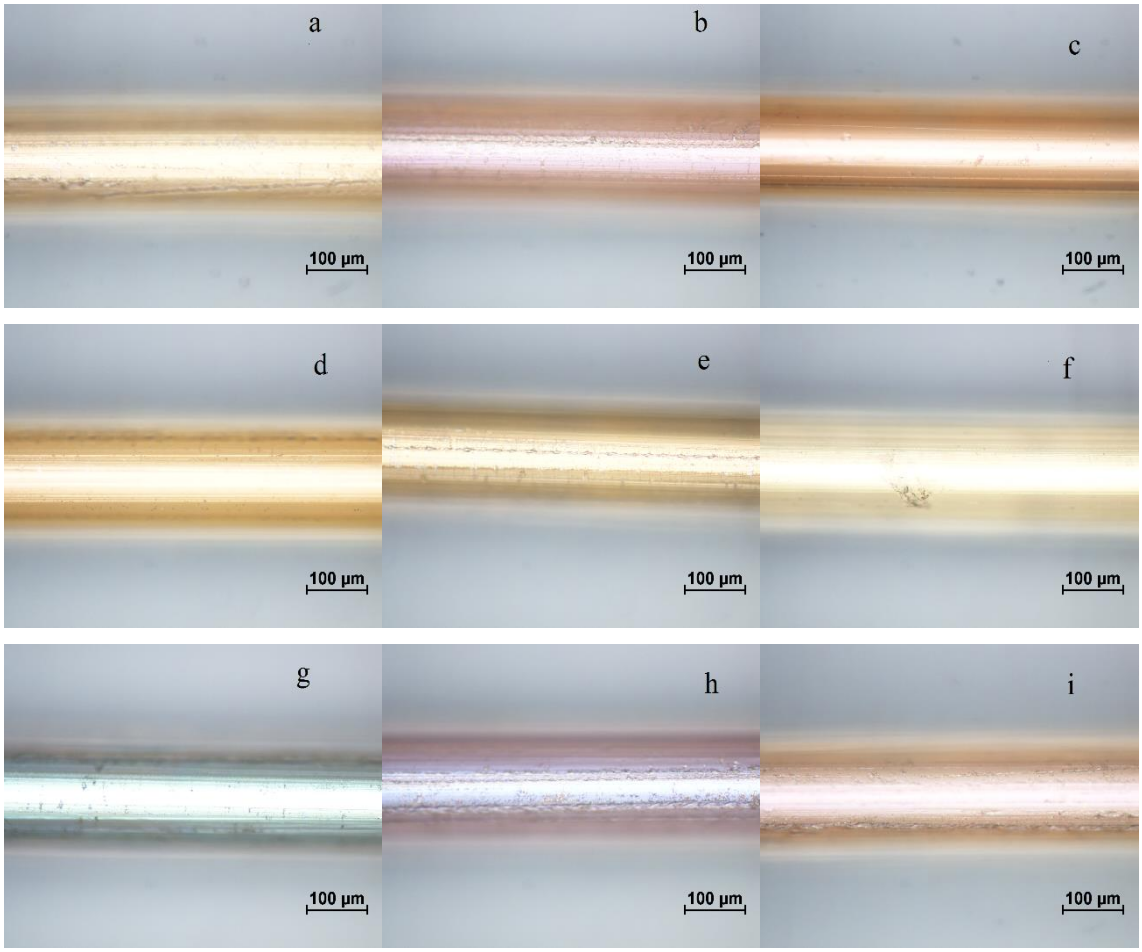

Figure 4.7. Optical microscopy images of ITO coated fiber

As it can clearly understood from the figure above, deposition parameters have significant effects on the optical properties of ITO coated polyamide fiber (This optical modulation is beyond of the scope of the thesis). Although the optical microscopy images show there is no much roughness but almost smooth surface, in order to achieve a certain conclusion scanning electron microscopy (SEM) should be performed.

Table 4.4. Deposition parameters of the ITO coated fibers in figure 4.5

Sample Name	a	b	c	d	e	f	g	h	i
Gas flow (sccm)	**100**	**100**	**100**	**100**	50	60	70	80	90
Deposition Pressure (10^{-3} torr)	4.7	4.7	4.7	4.7	4.1	4.3	4.6	4.9	4.9
Power (Watt)	80	90	100	110	**90**	**90**	**90**	**90**	**90**
Rotator Velocity (cm/min)	119	119	119	119	119	119	119	119	119

The SEM images of (b), (c), (e) and (f) are given in the figure 4.6, 4.7, 4.8 and 4.9 respectively.

4.2.2.2. Scanning Electron Microscopy (SEM) Results

In order to recognize the structure of the ITO coated fibers in detail, it might be useful investigating the SEM images of un-coated fiber first. See the figure below.

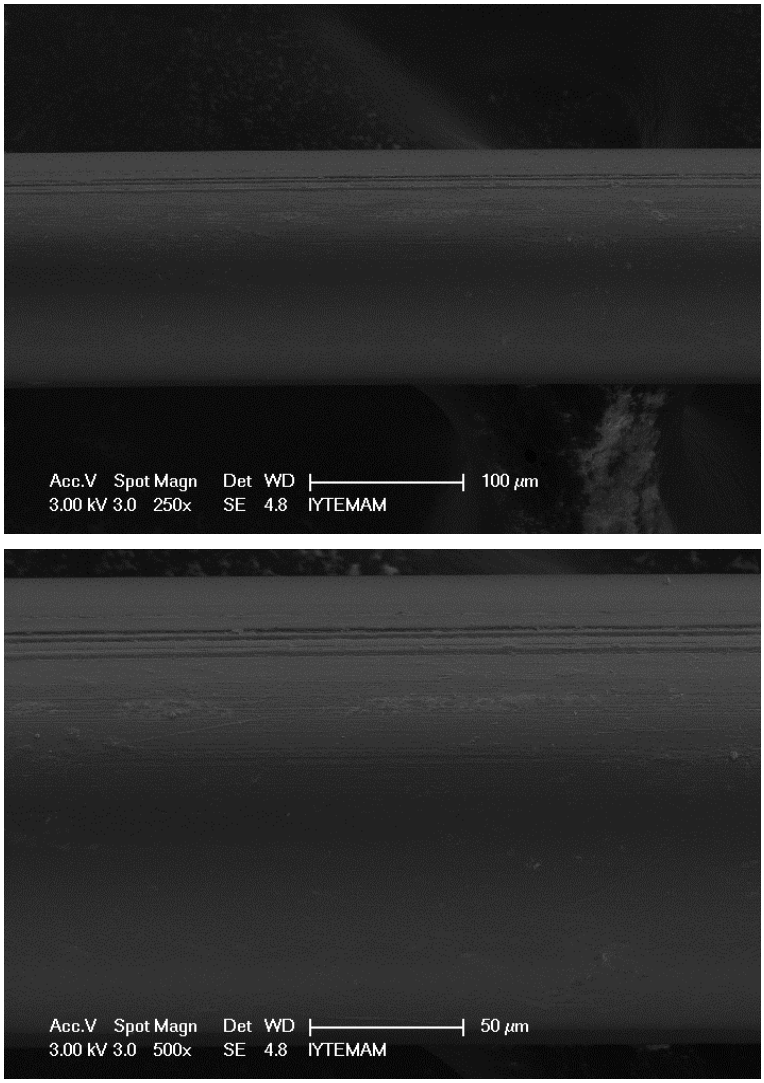

Figure 4.8. SEM images of un-coated fiber

Figure 4.8 shows the structure of the surface of the un-coated fiber is quite smoot and there is no cracks and no roughness.

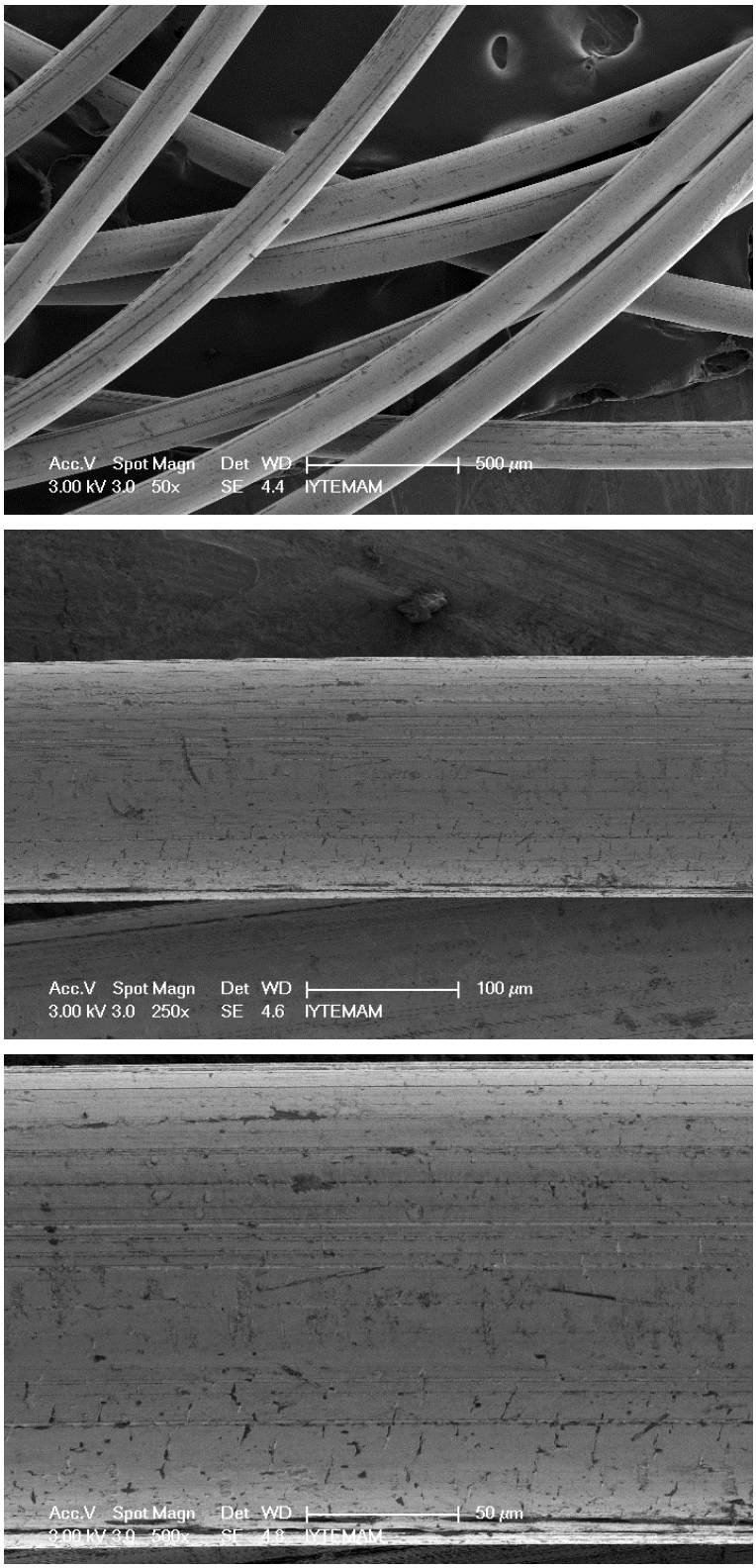

Figure 4.9. SEM images of ITO coated fiber (b).

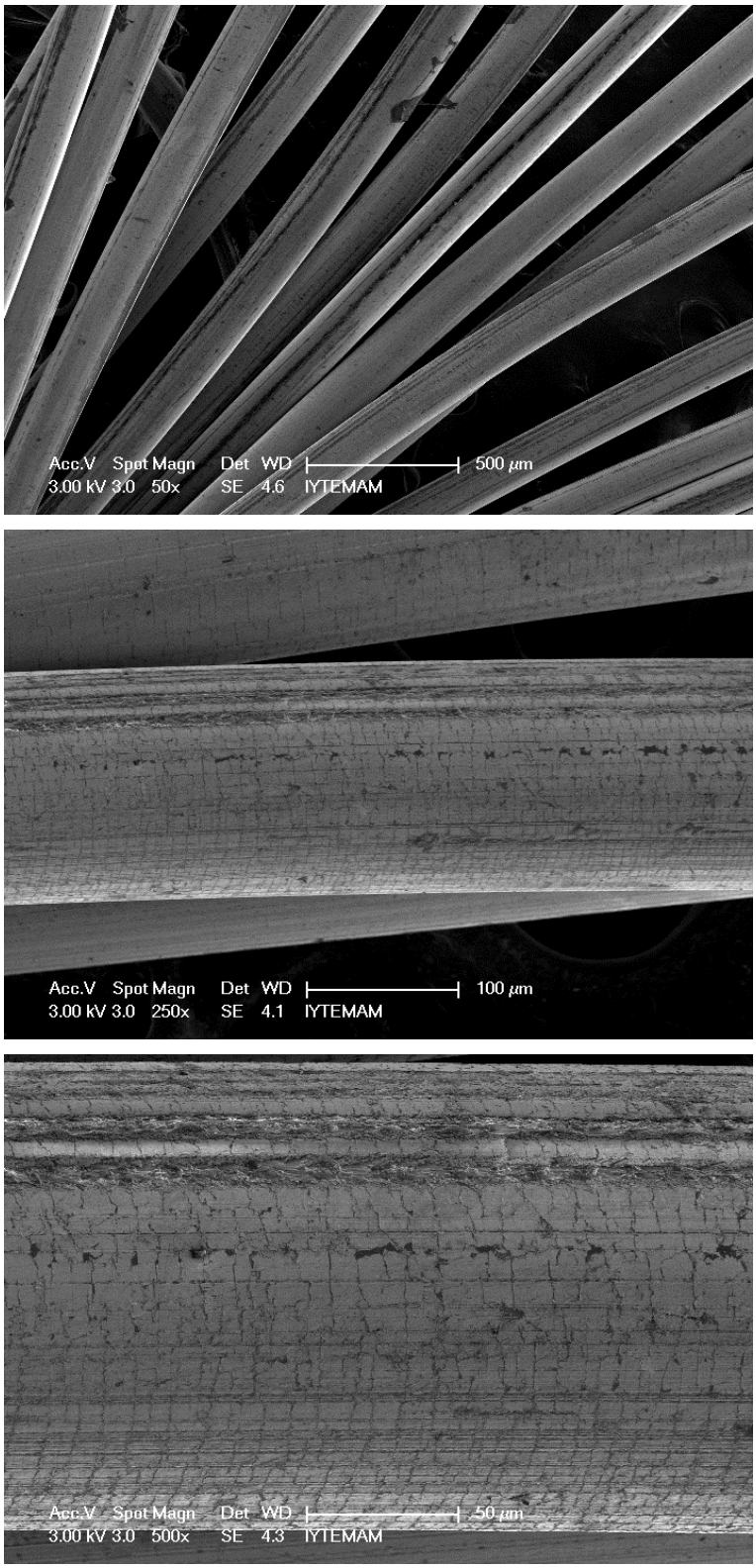

Figure 4.10. SEM images of ITO coated fiber (c).

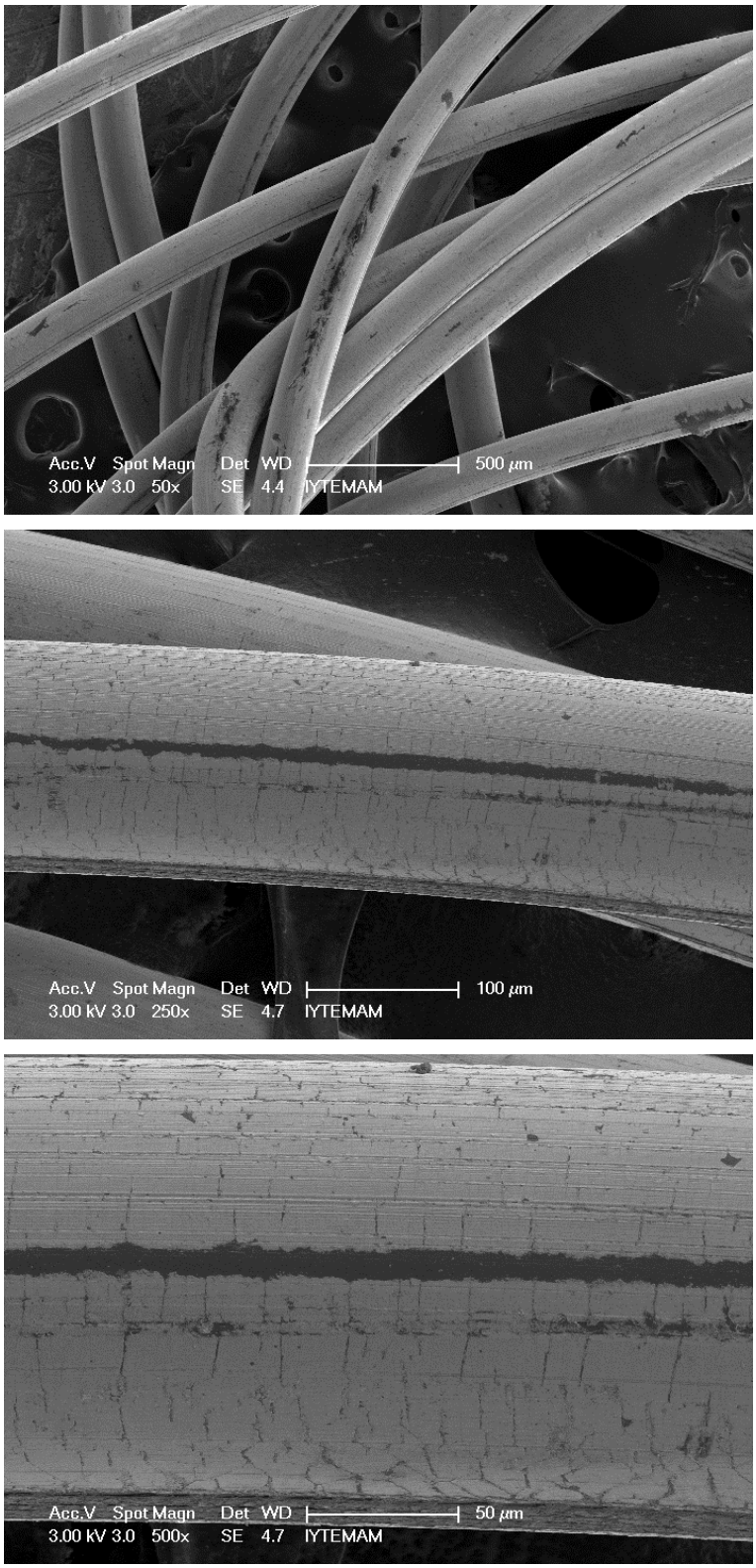

Figure 4.11. SEM images of ITO coated fiber (e).

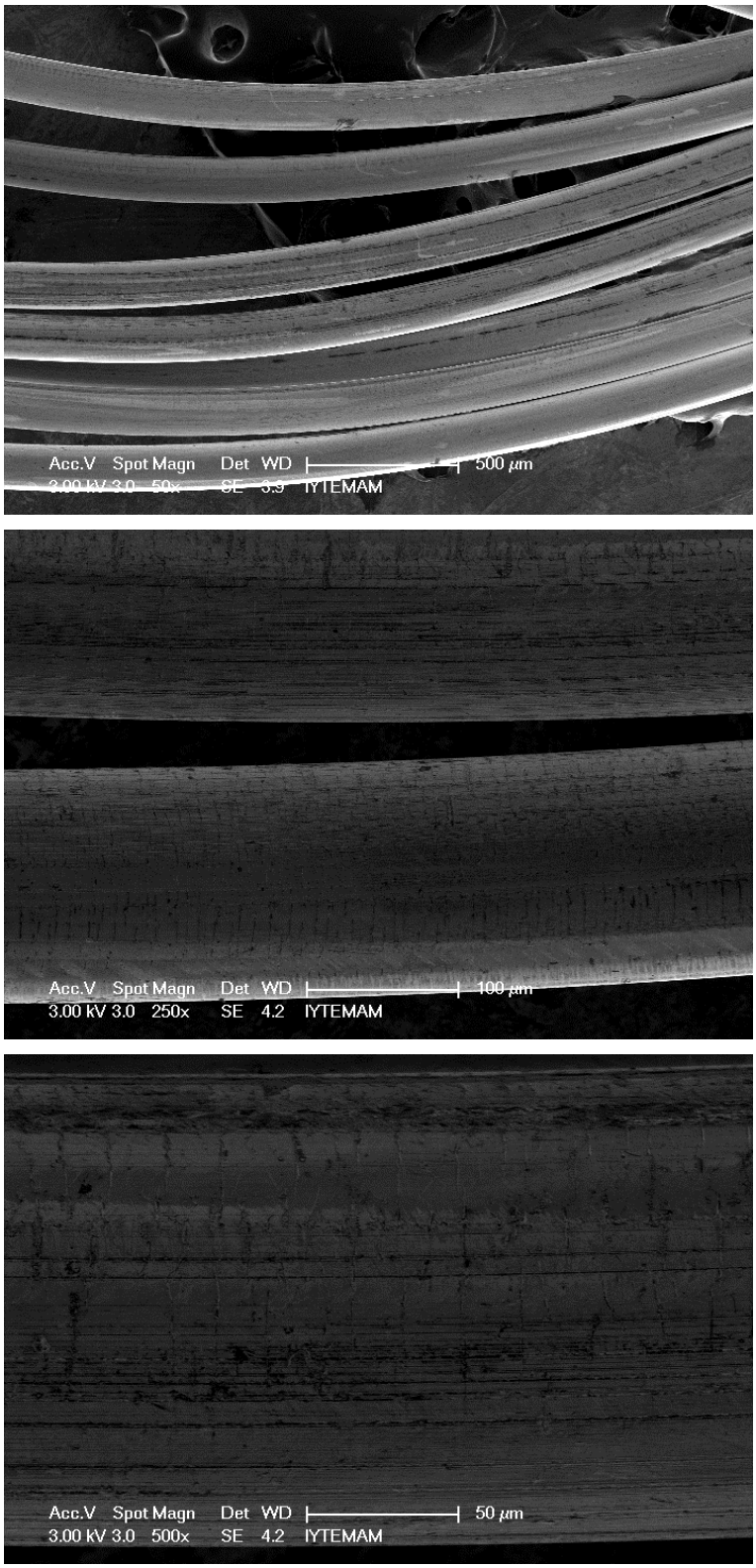

Figure 4.12. SEM images of ITO coated fiber (f).

As they might be clearly noticed from the SEM pictures, unlike optical microscopy images there are many cracks both on the horizontal axis and vertical axis on the surface of the fiber, resulting in lower electrical conductance (The electrical characterization is mentioned in the following section.). Although those cracks might be result from both the tensile strain of the fiber and the lower adhesion force between the ITO atoms and polyamide atoms. SEM images show the breadth-wise cracks are dominant, indicating the tensile strain has major role on the irregularity of the structure of the deposited ITO thin film.

4.3. Electrical Characterization Results

According to the scope of the thesis either the resistance and ionization gas pressure or the resistance and applied power relationship were analyzed by measuring resistance of each coated fiber which have different deposition parameters. The electrical measurements were repeated 10 times for each sample and the final electrical resistance is determined as the average of these values. The deposition parameters of fixed gas flow are given in table 4.5 while the electrical measurements of the samples are listed in table 4.6 with their standard deviations. The standard deviations have been calculated with the help of equation 4.1. The relative standard deviations have been calculated with the help of equation 4.2.

Table 4.5. Deposition parameters of ITO coated fiber for fixed gas flow.

Sample Name	l	m	n	a	b	c	d	p	r
Gas flow (sccm)	**100**	**100**	**100**	**100**	**100**	**100**	**100**	**100**	**100**
Deposition Pressure (10^{-3} torr)	4.7	4.7	4.7	4.7	4.7	4.7	4.7	4.7	4.7
Power (Watt)	**50**	**60**	**70**	**80**	**90**	**100**	**110**	**120**	**130**
Rotator Velocity (cm/min)	119	119	119	119	119	119	119	119	119

Table 4.6. Electrical measurements result for fixed gas flow.

Sample Name	r	p	d	c	b	a	n	m	l
Measurement 1 (kΩ / cm)	24.7	36.5	32.6	36.2	43.6	63.6	154.0	312.0	760.0
Measurement 2 (kΩ / cm)	31.0	39.0	31.2	30.8	50.0	62.0	173.2	298.7	763.0
Measurement 3 (kΩ / cm)	27.0	40.6	29.0	34.4	51.0	64.0	166.9	276.0	814.3
Measurement 4 (kΩ / cm)	28.3	31.3	28.3	33.0	53.0	67.4	152.1	283.6	823.0
Measurement 5 (kΩ / cm)	23.4	30.0	28.0	37.0	47.7	75.2	160.0	297.4	824.2
Measurement 6 (kΩ / cm)	26.0	32.7	33.8	28.6	55.4	78.0	187.0	332.3	777.8
Measurement 7 (kΩ / cm)	30.0	37.4	29.4	27.7	49.0	66.8	157.3	302.0	793.0
Measurement 8 (kΩ / cm)	26.6	39.5	33.0	34.3	53.0	69.0	152.7	317.5	798.7
Measurement 9 (kΩ / cm)	32.0	35.0	26.0	38.0	47.0	70.2	163.0	304.0	810.0
Measurement 10 (kΩ / cm)	21.0	38	38.7	30.0	60.3	63.8	173.8	276.5	856.0
Main Resistance (kΩ / cm)	**27.0**	**36.0**	**31.0**	**33.0**	**51.0**	**68.0**	**164.0**	**300.0**	**802.0**
Standard Deviation (kΩ / cm)	**3.2**	**3.4**	**3.4**	**3.4**	**4.4**	**5.0**	**10.6**	**17.0**	**28.3**
Relative Standard Deviation (RSD %)	**11.8**	**9.4**	**10.9**	**10.3**	**8.6**	**7.3**	**6.4**	**5.6**	**3.5**

Figure 4.13., 4.14., 4.15. Show the electrical resistance measurements of the data, which are given in the table above.

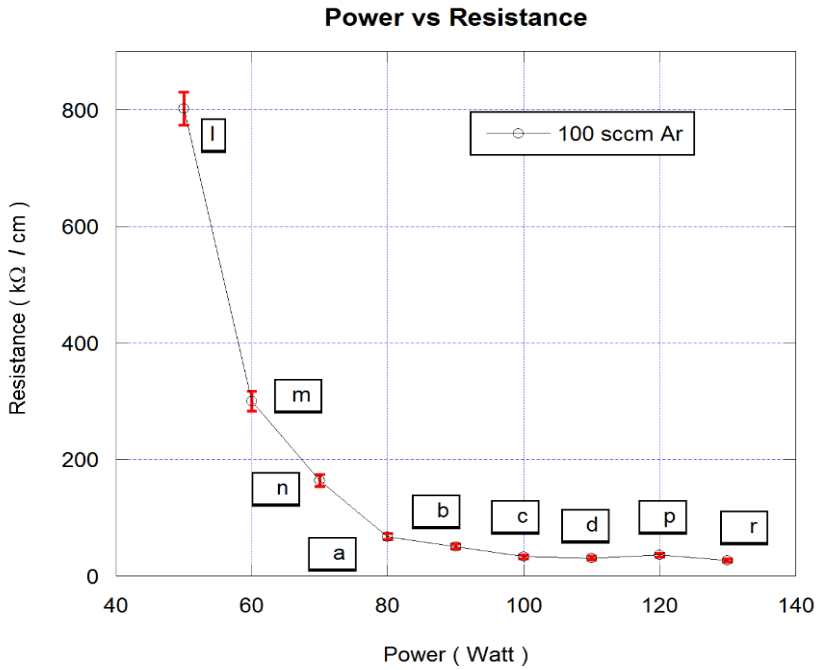

Figure 4.13. Resistance measurements results with respect to the gas flow.

As it might seen in the figure above the error bars are not discernible resulting from resistance scale difference. In order to solve that problem it will be useful separating the datas into two as in the figure 4.14. and 4.15.

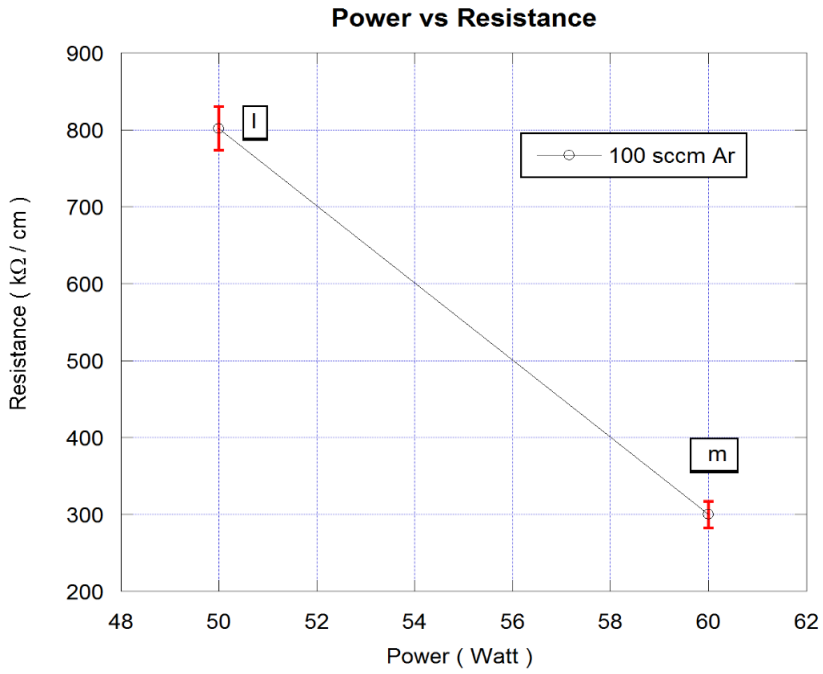

Figure 4.14. Resistance measurements results with respect to 50 and 60 W

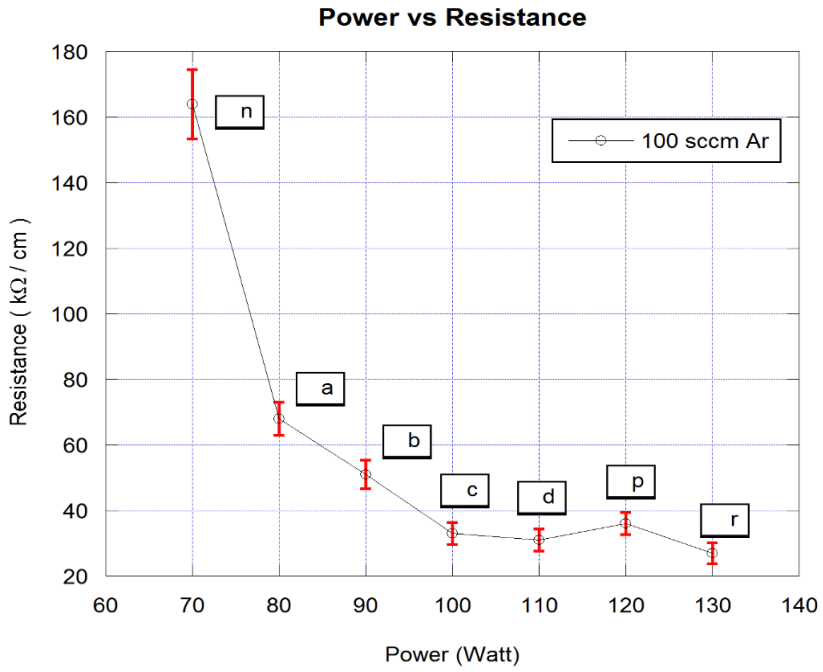

Figure 4.15. Resistance measurements results with respect to 70 - 130 W interval.

The deposition parameters of fixed power are given in table 4.7 while the electrical measurements of the samples are listed in table 4.8 with their standard deviations. The standard deviations have been calculated with the help of equation 4.1. The relative standard deviations have been calculated with the help of equation 4.2.

Table 4.7. Deposition parameters of ITO coated fiber for fixed power value.

Sample Name	i	h	g	f	e	k
Gas flow (sccm)	**90**	**80**	**70**	**60**	**50**	**40**
Deposition Pressure (10^{-3} torr)	5.4	4.9	4.6	4.3	4.1	4.1
Power (Watt)	**90**	**90**	**90**	**90**	**90**	**90**
Rotator Velocity (cm/min)	119	119	119	119	119	119

Table 4.8. Electrical measurements results for fixed power value.

Sample Name	k	e	f	g	h	i
Measurement 1 (kΩ / cm)	17.0	21.0	37.0	18.0	24.3	74.8
Measurement 2 (kΩ / cm)	16.4	21.7	34.5	18.9	20.0	76.0
Measurement 3 (kΩ / cm)	18.2	19.8	39.0	19.1	27.7	92.4
Measurement 4 (kΩ / cm)	19.0	20.0	31.5	19.3	19.0	82.0
Measurement 5 (kΩ / cm)	16.5	20.8	38.2	18.4	22.2	81.0
Measurement 6 (kΩ / cm)	17.2	22.0	39.8	18.7	20.8	79.6
Measurement 7 (kΩ / cm)	17.0	19.0	36.0	19.0	21.0	83.4
Measurement 8 (kΩ / cm)	19.0	19.8	33.3	18.4	22.0	87.0
Measurement 9 (kΩ / cm)	16.8	23.0	39.0	20.2	23.0	80.6
Measurement 10 (kΩ / cm)	15.9	25.9	41.7	17.0	20.0	93.2
Mean Resistance (kΩ / cm)	**17.3**	**21.3**	**37.0**	**18.7**	**22.0**	**83.0**
Standard Deviation (kΩ / cm)	**1.0**	**1.9**	**3.0**	**0.8**	**2.4**	**5.8**
Relative Standard Deviation (RSD %)	**5.7**	**8.9**	**8.1**	**4.2**	**10.9**	**6.9**

Electrical measurements of the data which are listed in the table above is giving in the figure 4.16.

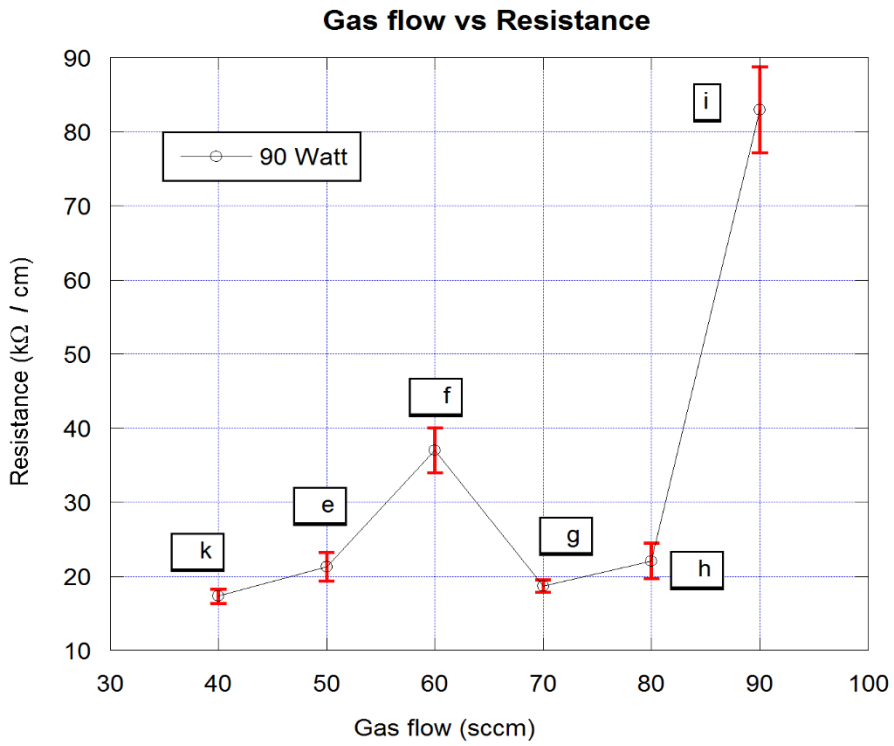

Figure 4. 16. Resistance measurements results with respect to gas flow.

The electrical characterizations indicate that the increase in power results in the reduction of the resistance of the thin film, which might be originated from the increment of the thickness of the thin film (The thickness of any TCO has inverse proportion with the resistance (Detailed information in chapter 2)). On the other hand, the increase in flow rate has negative effect on the resistance of thin film. This results might be explained either by the surface-particle interaction or momentum transfer which occurs between the sputtered atoms and ionization gas molecules in the environment. Power increase causes more energetic ions, which reduces both the number of the sputter atoms and kinetic energy of these sputtered atoms. This phenomenon result in the increment of the thin film thickness. But a positive change in the gas flow rate has quite negative effects on the quality of the film; the increase in the number of the ionized gas molecules causes more collision between sputtered target atoms and themselves. After many collisions sputtered atoms lose their kinetic energy that leads them to deposit on the surface resulting in low deposition rate.

4.4. Thickness Measurements Results

4.4.1. Thickness Measurements Results (Deposited ITO mass).

The measurements via deposited ITO mass can be done by running the formula, which is given in the section 3.6.2.1 with the help of the masses un-coated and ITO coated fibers:

10 meters un-coated PA fiber mass is 0.294 g whereas 10 meters ITO coated fiber mass is at the range of 0.298 g and 0.303 g which results in the alteration of the thin film thickness at the range of 307 and 516 nm.

Table 4.9.Thickness measurement of the films for fixed gas flow.

Sample name	r	p	d	c	b	a	n	m	l
thickness (nm)	443	431	423	398	384	392	377	342	313

Table 4.10. Thickness measurements of the thin films for fixed applied power.

Sample name	k	g	e	h	f	i
thickness (nm)	516	418	416	399	392	402

4.4.2. Thickness Measurements Results (SEM images).

By using the SEM images of coated and un-coated fibers, the thickness of the thin film can be measured.

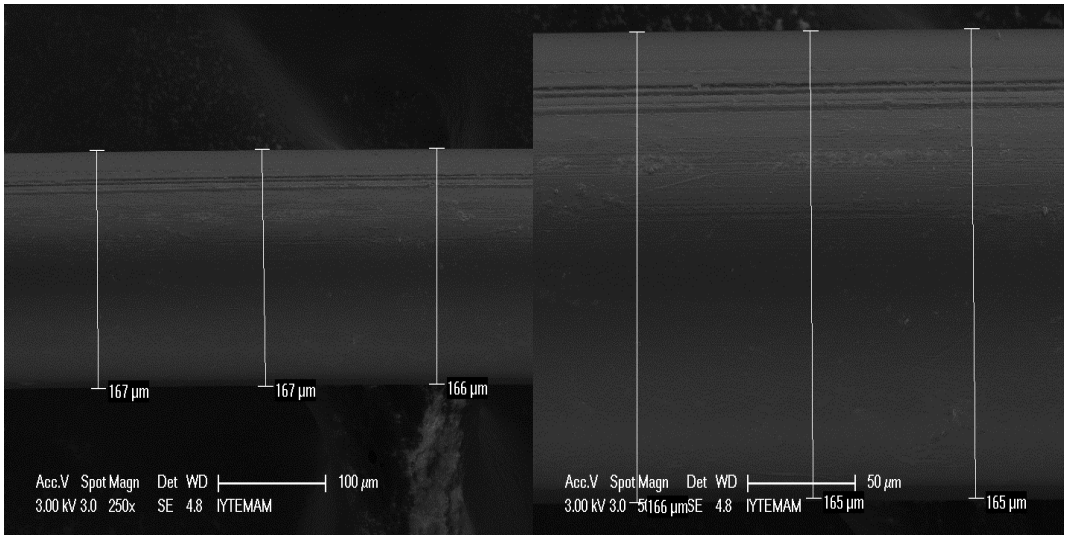

Figure 4.17. Thickness measurements of un-coated fiber from the SEM image.

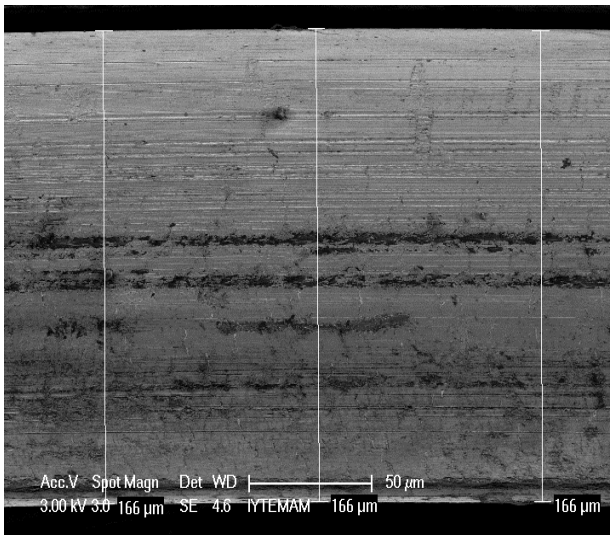

Figure 4.18.Thickness measurements of ITO coated fiber (d) from the SEM image.

SEM images show that, the thickness of the thin film is about 400 nm

4.4.3. Thickness Measurements Results (Calibration sample).

In this technique a piece of lamellae, which is shaped as fiber (0.5 cm width, 5 cm length), is located ICM plasma area and deposited with the same parameters. The results are listed in the table 4.11.

Table 4.11. Thickness measurements of calibration samples.

Sample name	k	c	b	a	f
thickness (nm)	452	408	396	502	516

As it might be noticed from the tables above, the adhesion force between ITO atoms and PA fiber atoms is not as good as the adhesion force between ITO atoms and glass atoms.

CHAPTER 5

CONCLUSION

After the exploration of CdO thin film by Baedeker in the beginning of 1900s, it was discovered that it was possible congregate the high electrical conductivity that the metals have and the high optical transparency features that the insulators have. These materials named as optical transparent conductive oxide (TCOs), have an extensive usage area from flexible monitors to OLEDs, solar panels to electrochromic structures, and particularly the transistors. ZnO, AlO, AZO, GAZO and ITO can be given as an example for optical transparent conductive oxides (Koseoglu et al. 2015). Due to its low electrical resistance and high optical transparency values, ITO is the most preferred TCO.

As the volume that the optical transparent conductive oxide thin films have, has been increasing day by day, it has led to the development of new coating methods. Even though these coating methods divided into two as chemical vapor deposition and physical vapor deposition (Chapter 2) have advantages and disadvantages in themselves, physical vapor deposition method comes to the forefront in terms of the homogeneity of film and the controllability of its quality. While thin film coating on planar surfaces (Generally glass surfaces are chosen) is possible thanks to the physical vapor deposition method, specialized systems are required in order to coat the surfaces that have geometrically different structures. In the scope of the thesis, specially designed roll to roll inverted cylindrical magnetron sputtering system was used to coat the cylindrical surfaces. After the designing, various trial runs were conducted for system polymer fiber coating (Literature scanning showed that there wasn't any article published on cylindrical polymer / polyamide. Optical microscopic images and electrical resistance measurements proved that it was possible to make ITO coating on polyamide fiber. After that, the studies were started by considering the dependence of the quality of magnified thin film on the ionized gas flow rate and on the energy applied (See chapter 2). At the first step of the experiments, studies were carried out with constant gas flow rate (100 sccm) and with the varying energy applied in each trial run (from 30 watts to 130 watts, with 10 watt steps).

As a result of these studies, parameters required for the lowest resistance value were determined; and as the second step, studies were carried out with the ionizing gas flow rate (from 40 sccm to 90 sccm with 10 sccm steps) for each experiment despite the constant energy amount. Surface analyses of the samples acquired were carried out by (SEM and optical microscope), thickness analyzes were carried out by (SEM images, by the mass of coated ITO, and by the measurements taken from the calibration samples by means of a profilometer), and electrical resistance values were calculated using a multi-meter. In consequence, it was observed that high energy application (~100 W) and low gas flow rate (~ 40 sccm) increased the quality of the film. Even though the thickness of the coating acquired (~ 410 nm) were applicable for the electrochromic structure (Monk et al. 2008) it was determined that the resistance values were high. As it can be understood from SEM images, this can be explained by the cracks (mostly horizontal) on the magnified thin film. The reason why the cracks were created, might be the tension applied on the fiber (the tension that occurs when the fiber is conveyed from one roll to another after coating). In addition to that, either not being able to anneal the fibers after deposition or not being able to heat the substrate during (before) deposition, can be given as the reason why it has high resistance due to it is known that the annealing process or heating during deposition have positive effects on the resistance (Koseoglu et al. 2015, Tuna et al. 2010).

REFERENCES

Baedeker, K. 1909. 'Über eine eigentümliche Form elektrischen Leitvermögens bei festen Körpern', Annalen der Physik, 334: 566-84.

Bashar, Shabbir A. 1998. 'Study of indium tin oxide (ITO) for novel optoelectronic devices', UMIST, Manchester: 106-09.

Boone, DH. 1986. 'Physical vapour deposition processes', Materials science and technology, 2: 220-24.

Cohen, Marvin L. 1998. 'Predicting new materials and their properties', Solid state communications, 107: 589-96.

Dawar, A. L., A. K. Jain, and C. Jagadish. Semiconducting transparent thin films. Bristol, UK, Philadelphia, PA: Institute of Physics Pub., 1995.

Diesing, D, AW Hassel, and MM Lohrengel. 1999. 'Aluminium oxide tunnel junctions: influence of preparation technique, sample geometry and oxide thickness', Thin Solid Films, 342: 282-90.

Facchetti, Antonio, and Tobin J Marks. 2010. 'Transparent electronics', From Synthesis to Applications, Wiley, Chichester, UK.

Fang, Te-Hua, and Win-Jin Chang. 2003. 'Effect of freon flow rate on tin oxide thin films deposited by chemical vapor deposition', Applied surface science, 220: 175-80.

Fuller, Lynn. 2011. 'Physical vapor deposition–evaporation and sputtering', Microelectronic Engineering Rochester Institute of Technology.

Ginley, David, Hideo Hosono, and David C Paine. 2010. Handbook of transparent conductors (Springer Science & Business Media).

Granqvist, Claes G. 1995. Handbook of inorganic electrochromic materials (Elsevier).

Hautier, Geoffroy, Anna Miglio, Gerbrand Ceder, Gian-Marco Rignanese, and Xavier Gonze. 2013. 'Identification and design principles of low hole effective mass p-type transparent conducting oxides', Nature communications, 4.

Kadlec, S, and J Musil. 1996. 'Low pressure magnetron sputtering and selfsputtering discharges', Vacuum, 47: 307-11.

Kern, Werner. 2012. Thin film processes II (Academic press).

Kim, Jun Young, Dong-Min Lee, Jae-Kwan Kim, Su-Hwan Yang, and Ji-Myon Lee. 2013. 'Effects of H 2/O 2 mixed gas plasma treatment on electrical and optical property of indium tin oxide', Applied surface science, 265: 145-48.

Koseoglu, Hasan, Fulya Turkoglu, Metin Kurt, Mutlu D Yaman, Fatime G Akca, Gulnur Aygun, and Lutfi Ozyuzer. 2015. 'Improvement of optical and electrical properties of ITO thin films by electro-annealing', Vacuum, 120: 8-13.

Maissel, Glang. 'Handbook of Thin Film TechnologyMcGraw-Hill (1970)', Chap, 16: 16.

Malherbe, JB, and RQ Odendaal. 1999. 'Ion sputtering, surface topography, SPM and surface analysis of electronic materials', Applied surface science, 144: 192-200.

Marezio, M. 1966. 'Refinement of the crystal structure of In2O3 at two wavelengths', Acta Crystallographica, 20: 723-28.

Mattox, DM. 1989. 'Particle bombardment effects on thin-film deposition: A review', Journal of Vacuum Science & Technology A, 7: 1105-14.

Mattox, Donald M. 2010. Handbook of physical vapor deposition (PVD) processing (William Andrew).

Minami, Tadatsugu. 2000. 'New n-type transparent conducting oxides', Mrs Bulletin, 25: 38-44.

Monk, Paul, Roger Mortimer, and David Rosseinsky. 2007. Electrochromism and electrochromic devices (Cambridge University Press).

Monk, Paul MS, Roger J Mortimer, and David R Rosseinsky. 2008. Electrochromism: fundamentals and applications (John Wiley & Sons).

Moshfegh, Alireza Zaker, HV Känel, SC Kashyap, and Matthias Wuttig. 2004. "Physics and Technology of Thin Films, Iwtf 2003." In Physics and Technology of Thin Films, IWTF 2003.

Moshfegh, AZ, HV Kanel, and SC Kashyap. 2004. Physics and Technology of Thin Films, Iwtf 2003: Proceedings of the International Workshop (World Scientific).

Nath, Prem, Rointan F Bunshah, BM Basol, and OM Staffsud. 1980. 'Electrical and optical properties of In 2 O 3: Sn films prepared by activated reactive evaporation', Thin Solid Films, 72: 463-68.

Ohring, Milton. 2001. Materials science of thin films (Academic press).

Özyüzer Lütfi, Zeynep MERİÇ, Yusuf SELAMET, Bengi KUTLU, and Aysun CİRELİ. 2010. 'Antistatic and Antibacterial Properties of Metal Coated Polypropylene Fibers by Magnetron Sputtering', 2010, The Journal of Textiles and Engineers (Volume: 17), 78.

Prenitzer, Brenda I. 2000. "Ion–Solid Interactions: Fundamentals and Applications, Michael Nastasi, James W. Mayer, and James K. Hirvonen, Cambridge University Press, 1996. ISBN 0-521-37376-X." In.: Elsevier.

Ramanathan, Shriram. 2010. 'Thin film metal-oxides', Harvard University: Springer New York Dordrecht Heidelberg London.

Rosendahl, Gottfried R. 1962. 'Contributions to the optics of mirror systems and gratings with oblique incidence. III. Some applications', JOSA, 52: 412-15.

Scanlon, David O. 2011. 'Electronic structure studies of p-type semiconducting oxides', Trinity College Dublin.

Seshan, Krishna. 2012. Handbook of thin film deposition (William Andrew).

Slocombe, Daniel, Adrian Porch, Michael Pepper, and Peter P Edwards. 2012. 'The Mott transition and optimal performance of transparent conducting oxides in thin-film solar cells', Energy & Environmental Science, 5: 5387-91.

Taşdemir, Adnan. 2015. 'Thin film coating of silver on fibers by roll to roll inverted cylindrical magnetron sputtering'. Department of Physics, Izmir Institute of Technology

Tilley, Richard JD. 2004. Understanding solids: the science of materials (John Wiley & Sons).

Tuna, Ocal, Yusuf Selamet, Gulnur Aygun, and Lutfi Ozyuzer. 2010. 'High quality ITO thin films grown by dc and RF sputtering without oxygen', Journal of Physics D: Applied Physics, 43: 055402.

Vogelzang, E, M Sikkens, and GA Sawatzky. 1986. 'Intrinsically selective absorption in alloys of early with late transition metals', Solar Energy Materials, 14: 365-73.

Wager, John F. 2003. 'Transparent electronics', Science, 300: 1245-46.

Wasa, Kiyotaka, and S Hayakewa. 1992. Handbook of Sputter Deposition (Noyes Publications, New Jersey).

Yamamura, Yasumichi, Yukikazu Itikawa, and Noriaki Itoh. 1983. 'Angular dependence of sputtering yields of monatomic solids'.